PLOS ONE

RESEARCH ARTICLE

Quantification of the neurochemical profile of the human putamen using STEAM MRS in a cohort of elderly subjects at 3 T and 7 T: Ruminations on the correction strategy for the tissue voxel composition

Ana Gogishvili[1,2,3☯], **Ezequiel Farrher**[1☯*], **Christopher E. J. Doppler**[4,5], **Aline Seger**[4,5], **Michael Sommerauer**[4,5], **N. Jon Shah**[1,6,7,8]

1 Institute of Neuroscience and Medicine 4, INM-4, Forschungszentrum Jülich, Jülich, Germany, **2** Faculty of Medicine, RWTH Aachen University, Aachen, Germany, **3** Engineering Physics Department, Georgian Technical University, Tbilisi, Georgia, **4** Cognitive Neuroscience, Institute of Neuroscience and Medicine 3, INM-3, Forschungszentrum Jülich, Jülich, Germany, **5** Department of Neurology, Faculty of Medicine and University Hospital Cologne, University of Cologne, Cologne, Germany, **6** Institute of Neuroscience and Medicine 11, INM-11, JARA, Forschungszentrum Jülich, Jülich, Germany, **7** JARA – BRAIN - Translational Medicine, Aachen, Germany, **8** Department of Neurology, RWTH Aachen University, Aachen, Germany

☯ These authors contributed equally to this work.
* e.farrher@fz-juelich.de

Citation: Gogishvili A, Farrher E, Doppler CEJ, Seger A, Sommerauer M, Shah NJ (2023) Quantification of the neurochemical profile of the human putamen using STEAM MRS in a cohort of elderly subjects at 3 T and 7 T: Ruminations on the correction strategy for the tissue voxel composition. PLoS ONE 18(6): e0286633. https://doi.org/10.1371/journal.pone.0286633

Editor: Federico Giove, Museo Storico della Fisica e Centro Studi e Ricerche Enrico Fermi, ITALY

Received: July 11, 2022

Accepted: May 19, 2023

Published: June 2, 2023

Data Availability Statement: The data are subject to some legal and ethical restrictions, which are also stated in the informed consent form approved by the Ethics Committee of the Medical Faculty of the University Cologne and signed by each participant. The general rules of the Forschungszentrum Jülich and the Ethics Committee of the Medical Faculty of the University Cologne provide the following procedure for the sharing of anonymised MRI data: Data may be

Abstract

The aim of this work is to quantify the metabolic profile of the human putamen *in vivo* in a cohort of elderly subjects using single-voxel proton magnetic resonance spectroscopy. To obtain metabolite concentrations specific to the putamen, we investigated a correction method previously proposed to account for the tissue composition of the volume of interest. We compared the method with the conventional approach, which *a priori* assumes equal metabolite concentrations in GM and WM. Finally, we compared the concentrations acquired at 3 Tesla (T) and 7 T MRI scanners. Spectra were acquired from 15 subjects (age: 67.7 ± 8.3 years) at 3 T and 7 T, using an ultra-short echo time, stimulated echo acquisition mode sequence. To robustly estimate the WM-to-GM metabolite concentration ratio, five additional subjects were measured for whom the MRS voxel was deliberately shifted from the putamen in order to increase the covered amount of surrounding WM. The concentration and WM-to-GM concentration ratio for 16 metabolites were reliably estimated. These ratios ranged from ~0.3 for γ-aminobutyric acid to ~4 for *N*-acetylaspartylglutamate. The investigated correction method led to significant changes in concentrations compared to the conventional method, provided that the ratio significantly differed from unity. Finally, we demonstrated that differences in tissue voxel composition cannot fully account for the observed concentration difference between field strengths. We provide not only a fully comprehensive quantification of the neurochemical profile of the putamen in elderly subjects, but also a quantification of the WM-to-GM concentration ratio. This knowledge may serve as a basis for future studies with varying tissue voxel composition, either due to tissue atrophy, inconsistent voxel positioning or simply when pooling data from different voxel locations.

shared with interested researchers whose identity and affiliation to a research institution must be ensured and confirmed. It must be made clear that the data will only be used by the interested researchers for research purposes in accordance with the provisions of the Declaration of Helsinki and in accordance with the provisions of the applicable data protection regulations (The General Data Protection Regulation). All data used for this publication is available upon request via the following contacts who can field data inquiries from fellow researchers: Secretary's office of the Institute of Neuroscience and Medicine (INM-4) Forschungszentrum Jülich: Wilma Fladung building: 15.14, room: 201 via phone (+49-2461-61-85575), fax (+49-2461-61-1919), and/or email (INM4-Sekretariat@fz-juelich.de).

Funding: AG was supported in part by the Shota Rustaveli National Science Foundation of Georgia (SRNSFG) [grant number - JFZ_18_02] (https://rustaveli.org.ge/geo). CEJD is supported by Clinician Scientist Program (CCSP), Faculty of Medicine, the University of Cologne (https://medfak.uni-koeln.de/en/), and is funded by the German Research Foundation (DFG, FI 773/15-1) (https://www.dfg.de/en/). MS is supported by the Else Kröner-Fresenius-Stiftung (grant number 2019_EKES.02) (https://www.ekfs.de/en). The funders had no role in study design, data collection and analysis, decision to publish, or preparation of the manuscript.

Competing interests: The authors have declared that no competing interests exist.

Abbreviations: 1H-MRS, proton magnetic resonance spectroscopy; Ala, alanine; Asc, ascorbate; Asp, aspartate; Cr, creatine; CRLB, Cramér-Rao lower bound; CSF, cerebrospinal fluid; FWHM, full width at half maximum; GABA, γ-aminobutyric acid; Glc, glucose; Gln, glutamine; Glu, glutamate; Glx, glutamate + glutamine; GM, grey matter; GPC, glycerophosphorylcholine; GSH, glutathione; Ins, *myo*-inositol; Lac, lactate; MM, macromolecules; NAA, *N*-acetylaspartate; NAAG, *N*-acetylaspartylglutamate; PCh, phosphorylcholine; PCr, phosphocreatine; PE, phosphorylethanolamine; PVE, partial volume effect; RF, radiofrequency; Scyllo, *scyllo*-inositol; SEM, standard error of the mean; SNR, signal-to-noise ratio; STEAM, stimulated echo acquisition mode; Tau, taurine; tCho, total choline; tCr, total creatine; TE, echo time; TM, mixing time; tNAA, total NAA; TR, repetition time; VOI, volume of interest; WM, white matter.

1. Introduction

Proton magnetic resonance spectroscopy (1H-MRS) enables the quantification of metabolite concentrations *in vivo*. It has proven to be a valuable tool for the assessment of several pathologies and disorders of the human brain, such as tumours [1], Alzheimer's disease [2, 3] and Parkinson's disease [4, 5], as well as for the study of healthy ageing [6, 7]. Although the added value of 1H-MRS is greatly enhanced if the metabolite concentration is provided in absolute units (e.g. moles per kilogram or litre of tissue), the majority of the clinical studies still make use of either relative concentrations (to total creatine (tCr) or total *N*-acetylaspartate (tNAA)) [8] or absolute concentrations without appropriate corrections (conventionally expressed in institutional units, [i.u.]) [9]. However, as concentrations of tCr and tNAA have been shown to change in certain brain pathologies [10] or even between brain regions [11], the applicability of this approach is clearly limited. The use of institutional units, on the other hand, restricts the use of the quantified concentrations to within studies, making it difficult to reproduce and compare results.

To achieve absolute quantification, several factors must be considered, including correction for signal relaxation and the use of a signal reference. The use of the unsuppressed tissue water signal as an internal reference has been shown to be of great value in quantifying the metabolic profile of the brain *in vivo* [12–15] since it enables the omission of certain correction factors, e.g. the radiofrequency (RF) field inhomogeneity. Techniques to account for the differences in tissue water concentration are widely used in research [8, 13, 16, 17]. Conversely, although the difference in metabolite concentration between white (WM) and grey (GM) matter has already been studied [18], the correction for such difference in the context of quantitative single-voxel MRS has received only minor attention [18–20]. This issue is particularly crucial for studies that include patients with brain atrophy [21] or in longitudinal studies where the positioning of the volume of interest (VOI) is not consistent [22]. Moreover, given the ubiquity of the partial volume effect (PVE) in single-voxel MRS, metabolite concentration ratios with the surrounding tissue also need to be accounted for when quantifying the metabolic profile of a specific brain structure. A possible mitigation of the problem with PVE in single-voxel MRS is to use the VOI tissue fractions as a covariate in the statistical analysis [21, 22]. However, a limitation of this approach is that the absolute metabolite concentration of the structure of interest remains unknown. An alternative approach was proposed by Harris et al. [19], in which, in addition to the conventional tissue-specific water concentration and signal relaxation, the WM-to-GM metabolite concentration ratio (termed from now on as the α_m-ratio) is explicitly considered. In particular, Harris et al. applied the method for quantifying the γ-aminobutyric acid (GABA) concentration in several brain areas, assuming a ratio of 0.5 (i.e., there is twice as much GABA in GM compared to WM). This approach was later shown to have a significant impact on the statistical analysis of GABA concentrations in healthy ageing: a significant dependency of GABA on age was observed if no correction was used, whereas the dependency was negligible if the α_m-ratio was considered [22]. Nonetheless, to the best of our knowledge, the method has not been applied to investigate other metabolites.

The primary goal of this study is to quantify the neurochemical profile of the human putamen *in vivo* using pre-existing experimental spectra from healthy control subjects. The data were acquired in a case-control study on Parkinson's disease using an ultra-short TE, single-voxel stimulated echo acquisition mode (STEAM) [23, 24] sequence at 3 Tesla (T) and 7 T [4]. The putamen was chosen due to its central role in the pathophysiology of Parkinson's disease.

Besides commonly applied corrections, such as transverse (T_2) and longitudinal (T_1) relaxation effects [25], we also considered the correction for the α_m-ratio [19]. This was achieved by first assessing the metabolite concentration α_m-ratio following the method proposed by Hetherington et al. [18]. The effect of incorporating the α_m-ratio into the correction method was then compared to the case where that feature was neglected. Finally, we compared the quantified neurochemical profiles achieved at 3 T and 7 T field strengths as a means of *in vivo* validation [25].

2. Materials and methods

2.1 Quantification methods

Both of the quantification methods we utilised make use of the unsuppressed water signal acquired from the same MRS voxel as the internal reference [13] and the concentration output from the software LCModel [26]. The conventional correction method (M_1) considers the metabolite concentration in CSF to be negligible compared to that of brain tissue. It takes into account that water concentration changes according to the tissue type [13, 27–29] and contains factors accounting for T_1 and T_2 relaxation effects in both the metabolite and water reference signals. The metabolite concentration in this case is written as follows [13, 25]:

$$c_{m,1} = A\,\frac{\sum_i c_{w,i} E^{(1)}_{w,i} E^{(2)}_{w,i} f_i}{E^{(1)}_m E^{(2)}_m (f_{GM} + f_{WM})} \tag{1}$$

where A is the metabolite concentration from LCModel [i.u.] (assuming the default relaxation and the water content correction factors in LCModel, ATTH2O and WCONC, equal 1), f_i are the tissue volume fractions within the VOI, and $c_{w,i}$ are the tissue water concentrations (i = WM, GM and CSF). Here we assume $c_{w,WM}$ = 36100 mM, $c_{w,GM}$ = 43300 mM, and $c_{w,CSF}$ = 53800 mM [13]. $E^{(1)}$ and $E^{(2)}$ are the T_1 and T_2 relaxation attenuation factors which, for the STEAM sequence, are [30]:

$$E^{(1)} = \left\{1 - \exp\left[\left(\frac{TE}{2} + TM - TR\right)\frac{1}{T_1}\right]\right\}\exp\left(-\frac{TM}{T_1}\right)$$

and

$$E^{(2)} = \exp\left(-\frac{TE}{T_2}\right),$$

where TM is the mixing time. $E^{(1)}$ and $E^{(2)}$ corrections can only be neglected when TR $\gg$ T_1, TM $\ll$ T_1 and TE $\ll$ T_2. Note that both relaxation terms for the metabolite case are assumed to be the same for WM and GM [13, 31, 32].

The second method (M_2) utilises the same corrections as in M_1, but with the additional consideration that metabolite concentrations in WM and GM may be different. The metabolite concentration can be written as [19]:

$$c_{m,2} = A\,\frac{\sum_i c_{w,i} E^{(1)}_{w,i} E^{(2)}_{w,i} f_i}{E^{(1)}_m E^{(2)}_m (f_{GM} + \alpha_m f_{WM})}, \tag{2}$$

where $\alpha_m = c_{WM}/c_{GM}$ is the WM-to-GM metabolite concentration ratio, and c_{WM} and c_{GM} are metabolite concentrations for pure WM and GM, respectively. Notice that $c_{m,2}$ in Eq (2) represents what the measured concentration would be if the VOI were entirely filled by GM [19].

2.2 Estimation of the concentration ratio α_m

The pure WM and GM metabolite concentrations, and consequently the concentration ratio, α_m, can be assessed by fitting a linear function to the concentration calculated with M_1 vs. the normalised GM volume fraction, $\varphi_{GM} = f_{GM}/(f_{GM}+f_{WM})$ [19]. The linear function can be expressed as

$$c_{m,1}(\varphi_{GM}) = (c_{GM} - c_{WM})\varphi_{GM} + c_{WM}, \quad (3)$$

where φ_{GM} lies in the range [0,1] and c_{GM} and c_{WM} are free parameters. Clearly, a sufficiently broad φ_{GM} range needs to be covered to achieve a robust estimation of c_{GM} and c_{WM}. However, most studies seek to position the VOI in a consistent manner throughout the subjects, inevitably leading to a rather small φ_{GM} range. Consequently, some works have opted to pool the data acquired from different voxel locations to achieve a more robust estimation of α_m [19, 33].

In order to consider the effect of a potential bias in the water relaxation times or tissue water content used in Eqs (1) and (2) in α_m, we evaluated the relative change, $\Delta\alpha_m$, as follows

$$\Delta\alpha_m = \frac{\alpha_m(b) - \alpha_m(b_0)}{\alpha_m(b_0)} \times 100\%, \quad (4)$$

where the parameter b can be either T_1, T_2, $c_{w,WM}$ or $c_{w,GM}$ and the subscript "0" denotes the unbiased counterpart. For the sake of simplicity, an equal bias in the water relaxation times for both WM and GM was assumed. Notice that due to the intrinsic assumption of non-distinct metabolite relaxation times between WM and GM in Eq (1), a bias in the metabolite relaxation times will not affect $\Delta\alpha_m$.

Finally, to investigate the way in which a possible bias in the estimated concentration ratio propagates into the metabolite concentration obtained following M_2, we defined the error, ε, in the absolute concentration if the concentration ratio used, i.e. α_m, differs from the actual concentration ratio, $\alpha_{m,0}$, as follows:

$$\varepsilon = \frac{c_{m,2}(\alpha_m) - c_{m,2}(\alpha_{m,0})}{c_{m,2}(\alpha_{m,0})} \times 100\%. \quad (5)$$

2.3 Subjects

MRS spectra were acquired from the putamen of 15 healthy subjects (age 53 to 80 years, mean 67.7 ± 8.3 years, six females and nine males) in the framework of a case-control Parkinson's disease study [4]. Due to the limited range of φ_{GM} in the MRS voxels of that study, five more age-matched subjects (three VOIs each) were measured. For these subjects, the VOI was deliberately shifted to include higher fractions of WM (see Section 2.4 *MR protocol*). The Parkinson's disease study was approved by the Ethics Committee of the Medical Faculty of the University of Cologne, Germany. The five extra subjects were measured under the approval of the Ethics Committee of the Medical Faculty of the RWTH Aachen University, Germany. All participants gave written informed consent according to the Declaration of Helsinki.

2.4 MR protocol

For all subjects, spectra were initially acquired on a Siemens 3 T hybrid PET/MR Tim Trio scanner (Siemens Medical Solutions, Erlangen, Germany) and then on a Siemens 7 T Terra

scanner. The 3 T scanner was equipped with a birdcage transmit coil and an 8-channel receive coil provided by the vendor, whereas the 7 T scanner used a single transmit coil with a 32-channel receive coil (Nova Medical, USA). The MPRAGE sequence [34] was used to position the VOIs in the putamen at 3 T. The protocol parameters were: TR = 2.5 s; TE = 2.89 ms; voxel-size = 1 × 1 × 1 mm^3; matrix-size = 176 × 232 × 256; flip angle, 7°. At 7 T, the MP2RAGE sequence [35] was utilised for the same purpose. The protocol parameters were: TR = 4.5 s; TE = 1.99 ms; voxel-size = 0.75 × 0.75 × 0.75 mm^3; matrix-size = 208 × 300 × 320; flip angle, 5°.

First- and second-order B0 shimming at the VOI was performed using FASTESTMAP [36], and the RF power was calibrated for each subject [37, 38]. Water suppression was achieved with VAPOR and was interleaved with outer volume suppression (OVS) [23, 39]. Spectra were measured using the STEAM sequence [6, 23], with the voxel centred in the left putamen. The protocol parameters at 3 T were: TE / TR / TM = 6 / 4800 / 47.8 ms; 128 averages; voxel-size = 21 (left-right) × 35 (anterior-posterior) × 21 (rostral-caudal) mm^3; receive-bandwidth, 2000 Hz; vector-size = 2048; flip angle = 90˚; RF pulse duration = 1920 μs. At 7 T, the protocol parameters were: TE / TR / TM = 4 / 8000 / 28 ms, 72 averages; voxel-size = 14 (left-right) × 32 (anterior-posterior) × 17 (rostral-caudal) mm^3; receive-bandwidth, 6000 Hz; vector-size = 2048; flip angle = 90˚; RF pulse duration = 1920 μs. One extra complete phase cycle was measured without the water suppression RF pulses for eddy-current correction and absolute quantification. The same 3 T and 7 T MRS protocols were also used for the five additional subjects, for whom three different voxel positions were measured, namely occipital (WM_1), parietal (WM_2), and frontal (WM_3) WM (S1 Fig).

2.5 Data preprocessing and quantification

All data sets from the 3 T and 7 T scanners were processed following the same pipeline with the help of the FID-A package [40], available for Matlab (Natick, MA, USA). The preprocessing steps included i) automatic detection and removal of motion corrupted scans [40] and ii) phase and frequency drift correction of individual averages using spectral registration in the frequency domain [41]. Analysis of the preprocessed data was performed using LCModel (6.3-1R) with the water scaling and eddy-current correction options enabled. Fitting was performed in the chemical shift range of 0.2 ppm to 4.2 ppm. The metabolite basis sets were generated with the help of the tool VeSPA [42] using the density matrix formalism [43] with ideal RF pulses and actual sequence timings [44, 45]. Both basis sets included spectra of 19 metabolites: alanine (Ala), ascorbate (Asc), aspartate (Asp), creatine (Cr), GABA, glucose (Glc), glutamine (Gln), glutamate (Glu), glutathione (GSH), glycerophosphorylcholine (GPC), *myo*-inositol (Ins), lactate (Lac), NAA, *N*-acetylaspartylglutamate (NAAG), phosphocreatine (PCr), phosphorylcholine (PCh), phosphorylethanolamine (PE), *scyllo*-inositol (Scyllo), taurine (Tau). Macromolecular spectra measured using the inversion recovery STEAM sequence at 3 T (TE = 8 ms) and 7 T (TE = 6 ms) available at MM Consensus Data Collection (https://github.com/mrshub/mm-consensus-data-collection), were additionally used in the basis sets [24, 46]. The default rigidity parameter was used for the baseline in LCModel (DKNTMN = 0.15). A metabolite was considered to be reliably estimated if measured in at least 50% of the subjects with a Cramér-Rao lower bound (CRLB) value less or equal to 50% [47, 48]. Only spectra with the LCModel full width at half maximum output (FWHM) lower than 0.07 ppm were considered. Moreover, if the correlation coefficient between two metabolites was less than -0.7, only their sum was reported (e.g. tCho [GPC+PCh] and tCr [Cr+PCr]), whereas both the total concentration and the individual concentrations (e.g. tNAA [NAA+NAAG]) were reported for metabolites showing a correlation of between -0.7 and -0.3 [47, 48].

2.6 Tissue segmentation

An important issue in metabolite quantification, as well as in the estimation of the α_m-ratio, is the tissue segmentation approach [19]. In contrast to cortical segmentation, which assumes the same structural features for the whole cortex, segmentation of subcortical structures requires methods that are specific to these structures [49]. Traditional methods, such as FAST [50], face problems with the segmentation of subcortical GM in single contrast images, e.g. the T_1-weighted images in this work, due to its limited contrast with WM. Therefore, given that the putamen VOI in our study contains both cortical and subcortical GM, in order to assess the tissue volume fractions, we utilised a combined approach in which FAST was used for the segmentation of cortical GM, WM, and CSF, and FIRST [51] was used for subcortical GM. Both tools are available as part of FSL (FMRIB Software Library v6.0.3).

2.7 Statistical analysis

Prior to the estimation of the α_m-ratio, the distributions of metabolite concentrations evaluated using M_1 ($c_{m,1}$) were compared between the scanners. If $c_{m,1}$ concentrations at 3 T vs. 7 T were not significantly different, then the pooled $c_{m,1}$ concentrations (3 T and 7 T) were used for the estimation of the α_m-ratio. Otherwise, 3 T and 7 T $c_{m,1}$ were considered separately, and the α_m-ratio was estimated for each field strength. A one-way analysis of covariance (ANCOVA) was used to compare the $c_{m,1}$ concentrations between the scanners, where φ_{GM} at each scanner was used as the covariate. This was performed with the help of the SPSS software (28.0.1.0 (142)).

The metabolite concentrations obtained using the correction methods M_1 and M_2 were compared for each field strength separately. To this end, a two-sample t-test was performed for each group of subjects. Additionally, a scanner comparison was performed for each of the correction methods utilising a two-sample t-test.

A further evaluation of the effect of using the α_m-ratio method (M_2) compared to the case of neglecting it (M_1) was performed by calculating the Pearson's correlation coefficient of the concentrations $c_{m,1}$ (and $c_{m,2}$) vs. φ_{GM}. While a significant correlation of $c_{m,1}$ vs. φ_{GM} for a given metabolite denotes that $\alpha_m \neq 1$ (i.e. different WM and GM concentrations), a lack of a correlation of $c_{m,2}$ vs. φ_{GM} for the same metabolite signifies that the use of method M_2 can indeed remove the dependence of the absolute metabolite concentration on the tissue voxel composition.

3. Results

3.1 Tissue segmentation

Fig 1 depicts the MRS voxel position and corresponding tissue segmentation for a representative subject from the putamen group measured at 3 T (top row) and 7 T (bottom row). The volume fractions averaged across subjects are shown in Table 1. Likewise, the fraction of putamen covered by the MRS voxel was 0.89 ± 0.03 (3 T) and 0.76 ± 0.04 (7 T). The corresponding VOI position of the WM voxels is shown in S1 Fig.

3.2 Water linewidth and spectral quality

Fig 2 shows the correlation between the linewidth of the unsuppressed water signals (i.e. FWHM of the water peak estimated with the help of the FID-A package [40]) acquired at both field strengths. The Pearson's correlation coefficient of the linewidth values at 3 T vs. 7 T was $r = 0.83$; $p < 10^{-7}$. The mean linewidth values for the putamen, averaged across subjects, were 0.077 ± 0.008 ppm (3 T) and 0.07 ± 0.01 ppm (7 T), 0.052 ± 0.005 ppm (3 T) and

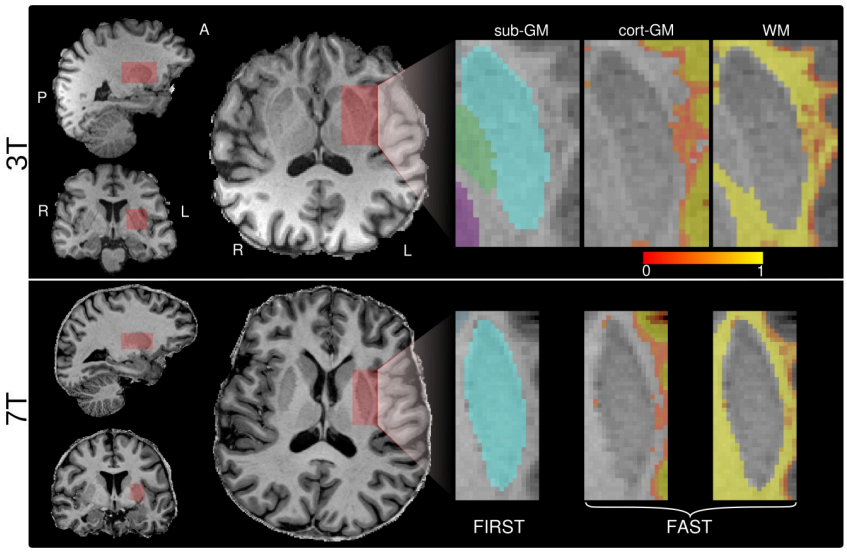

Fig 1. Examples of the putamen VOI positioning at 3 T (top panel) and 7 T (bottom panel) overlaid to the respective anatomical images. Tissue segmentation using FIRST for subcortical structures and FAST for cortical GM and WM are depicted. In the case of subcortical GM, the colours refer to: light blue, putamen (PUT); green, globus pallidus; violet, thalamus. In the case of FAST, the colour scale refers to the cortical GM/WM volume fraction.

https://doi.org/10.1371/journal.pone.0286633.g001

0.05 ± 0.01 ppm (7 T) for occipital WM, 0.064 ± 0.008 ppm (3 T) and 0.054 ± 0.009 ppm (7 T) for parietal WM, and 0.057 ± 0.004 ppm (3 T) and 0.05 ± 0.01 ppm (7 T) for frontal WM.

A mean of 6.9 averages (5.4% of the number of averages) were discarded from the total number of averages at 3 T, whereas at 7 T, a mean of 2.4 (3.3%) averages were discarded. The spectral characteristics of the putamen VOI at 3 T (left column) and 7 T (right column) are depicted in Fig 3. The mean (grey, solid line) and standard deviation (grey, shaded area) of the measured spectra taken over the subjects in the putamen group are shown at the top of the figure. Additionally, the individual spectra for both scanners are shown in S2 Fig. Single spectra (black, solid lines), together with the corresponding LCModel fit (red, solid line), the residuals, and the individual metabolite contributions are additionally shown for a representative subject. The random distributions of the residuals indicate a good fitting of the spectra achieved with LCModel at both field strengths. A total of 12 metabolites and four total concentrations (tCho, tNAA, tCr, and Glx (Gln+Glu)) were reliably measured following the conditions described in Section 2.5. In the case of the pairs Cr-PCr and GPC-PCh, the correlation was < -0.7 for both field strengths, whereas for the pair NAA-NAAG the mean correlation was equal

Table 1. Mean and standard deviation of the VOI tissue composition across subjects.

	WM	GM	CSF
PUT 3 T	0.37 ± 0.02	0.60 ± 0.03	0.03 ± 0.01
PUT 7 T	0.34 ± 0.06	0.66 ± 0.06	0.003 ± 0.002
WM_1 3 T	0.87 ± 0.04	0.10 ± 0.04	0.03 ± 0.01
WM_1 7 T	0.95 ± 0.03	0.04 ± 0.02	0.01 ± 0.01
WM_2 3 T	0.62 ± 0.09	0.35 ± 0.11	0.03 ± 0.01
WM_2 7 T	0.74 ± 0.13	0.25 ± 0.12	0.01 ± 0.12
WM_3 3 T	0.82 ± 0.07	0.13 ± 0.05	0.05 ± 0.02
WM_3 7 T	0.88 ± 0.06	0.10 ± 0.04	0.02 ± 0.02

https://doi.org/10.1371/journal.pone.0286633.t001

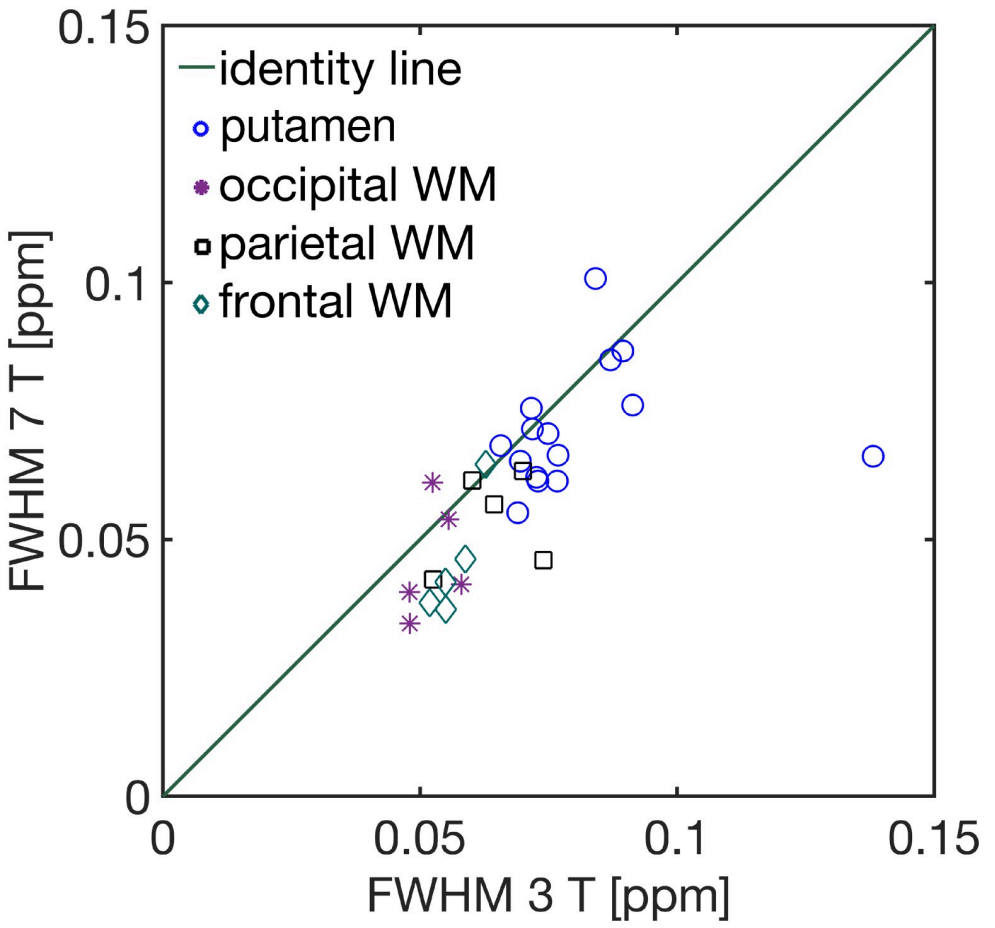

Fig 2. Linewidth of the unsuppressed water signal for the individual subjects achieved at 3 T vs. 7 T. ○: putamen; *: occipital WM; □: parietal WM; ♢: frontal WM. Note that the subject with linewidth 0.14 ppm was excluded from the correlation due to poor B0 shimming.

https://doi.org/10.1371/journal.pone.0286633.g002

to -0.65 (3 T) and -0.49 (7 T). Scyllo was only reliably detected at 3 T. The average signal-to-noise ratio (SNR) values obtained with LCModel (defined as the ratio of the maximum in the spectrum minus the baseline to twice the root-mean-square of the residuals) were 31 ± 3 at 3 T and 34 ± 9 at 7 T. The metabolite concentrations as outputted by LCModel without further corrections averaged over the whole putamen group for both scanners are indicated in S1 Table.

3.3 Concentration ratio α_m

Fig 4 shows the metabolite concentrations quantified using method M_1 (Eq (1)), $c_{m,1}$, plotted against the normalised volume fraction, φ_{GM}. The water and metabolite relaxation times used in Eqs (1) and (2) are indicated in S2 Table. The ANCOVA analysis using φ_{GM} as the covariate showed that the $c_{m,1}$ distributions of Gln, tCr, and Glx were significantly different ($p < 0.05$) between field strengths. Therefore, the α_m-ratio values for these metabolites were estimated separately for each field strength (red and blue lines in Fig 4). For the rest of the metabolites, only one α_m-ratio value per metabolite was estimated using the pooled data (green lines in Fig 4). In both cases, the α_m-ratio was estimated via linear regression of Eq (3).

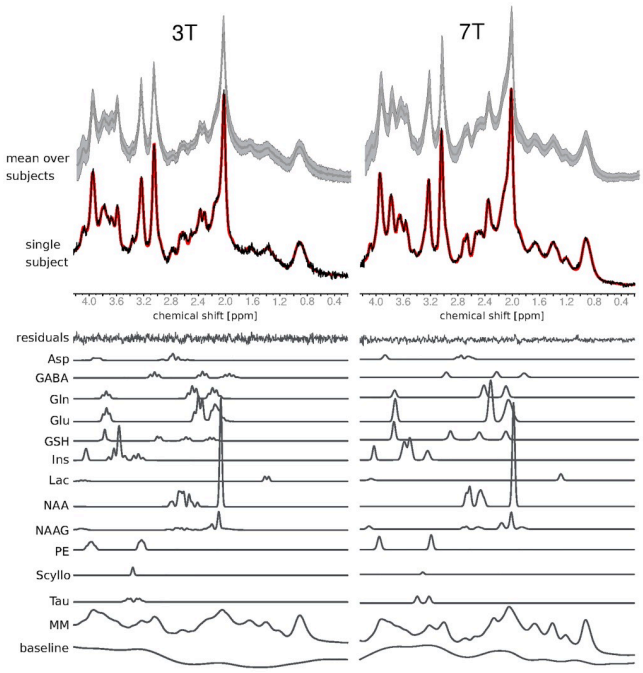

Fig 3. Top: mean (grey, solid line) and standard deviation (grey, shaded area) of the experimental spectra obtained from the putamen at 3 T (left) and 7 T (right). The spectra of a representative subject (black, solid line) are shown overlaid to the corresponding LCModel fit (red, solid line) together with the corresponding residuals of the fit. The individual metabolite contribution to the total spectra obtained with LCModel is additionally shown at the bottom of the figure.

https://doi.org/10.1371/journal.pone.0286633.g003

Table 2 shows the α_m-ratio values estimated in this work, along with literature values as a reference (or the range of values, if available). The putamen mean and standard error of the mean (SEM) metabolite concentrations calculated with the correction method M_2 are also summarised in Table 2. Additionally, the CRLB values for each field strength are reported.

Fig 5 depicts the parameter $\Delta\alpha_m$ evaluated using Eq (4), where the changes in b were evaluated according to $\Delta b = (100\% \times (b - b_0)/b_0$. The parameter $\Delta\alpha_m$ was assessed for several values of ΔT_1, ΔT_2, $\Delta c_{w,WM}$ and $\Delta c_{w,GM}$ ranging from -20% to +20%. For the case of the water relaxation times, $\Delta\alpha_m$ was evaluated for a range of TE, TR, and TM values (Fig 5a–5h). In the particular case of the water relaxation times and for the TR, TE, and TM used in our experiments, the resulting values of $\Delta\alpha_m$ for the 3 T scanner lie in the range between -0.17% and 0.18%, whereas the for the 7 T scanner the values of $\Delta\alpha_m$ lie in the range between -0.7% and 0.9%. That is to say, based on our experimental parameters, a bias of ±20% in either of the water relaxation times would result in $\Delta\alpha_m < 1\%$. On the contrary, Fig 5i shows that the parameter $\Delta\alpha_m$ is much more sensitive to a change in the tissue water content.

Table 3 shows the Pearson's correlation coefficients (ρ) and p-values of $c_{m,1}$ and $c_{m,2}$ vs. φ_{GM} for each metabolite. As expected, concentrations $c_{m,1}$ show a high correlation ($p < 0.05$) with φ_{GM}, for metabolites whose WM and GM concentrations are notoriously different. However, $c_{m,2}$ concentrations show no correlation with φ_{GM} ($p > 0.05$) in any metabolites, highlighting the ability of M_2 to remove the dependence of the concentration on φ_{GM}.

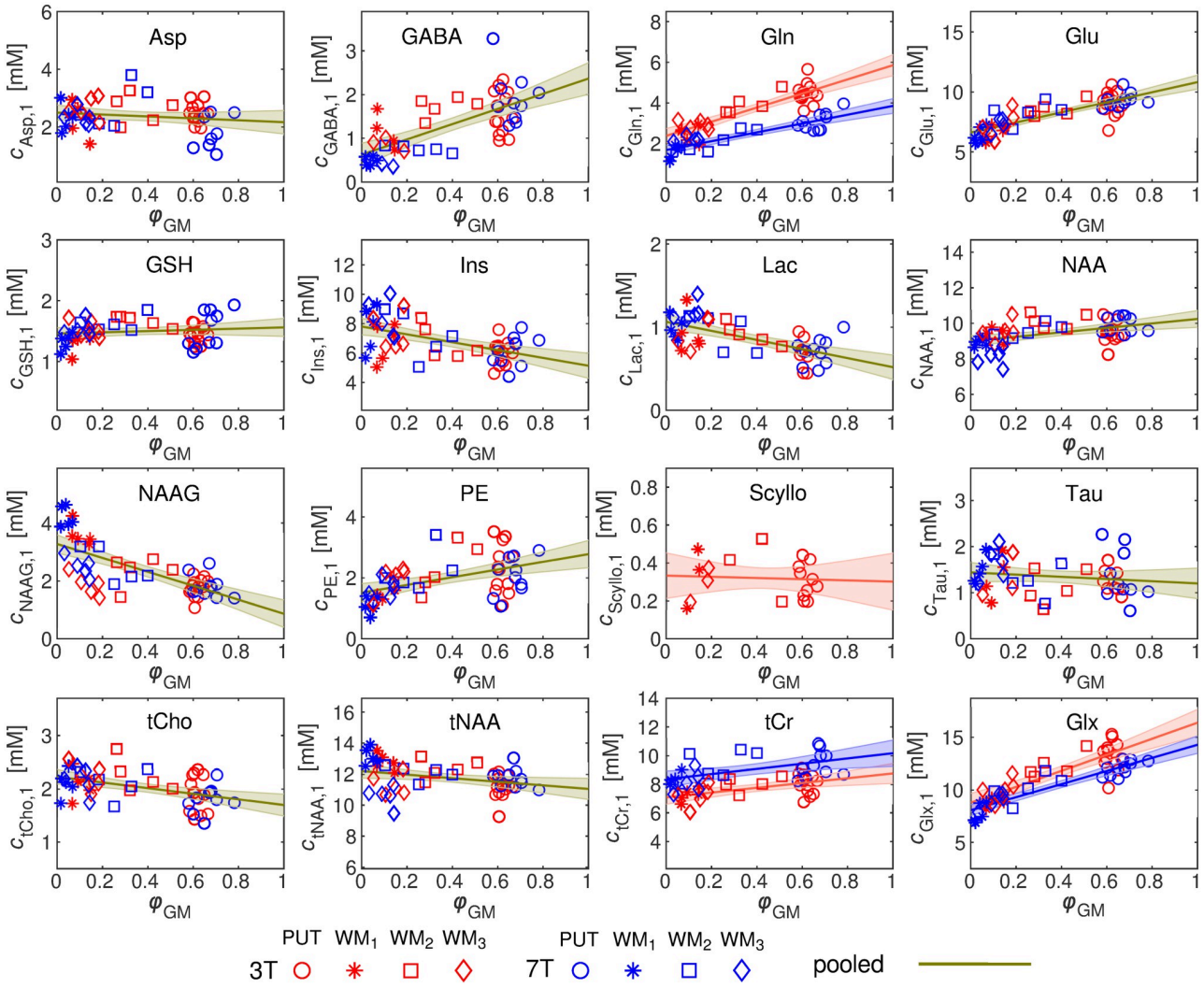

Fig 4. Plots of the $c_{m,1}$ concentrations vs. φ_{GM} for 3 T (red) and 7 T (blue) data, and for the whole metabolic profile. The regression lines (solid lines, Eq (3)), together with the 95% confidence bands (shaded areas), are additionally shown. Note that Gln, tCr and Glx distributions were significantly different between the scanners, as assessed by the ANCOVA analysis using φ_{GM} as the covariate ($p < 0.05$). Therefore, the linear regression was performed separately for 3 T (red line) and 7 T (blue line) for these metabolites. For the rest of the metabolites, the linear regression (green lines) was performed using the pooled data. All brain areas were considered for the linear regression. o: putamen (PUT); *: occipital WM; □: parietal WM; ♢: frontal WM.

https://doi.org/10.1371/journal.pone.0286633.g004

3.4 Effect of a bias in α_m values in method M_2

Fig 6a–6c shows the simulated error, ε (Eq 5), as a function of the concentration ratio, α_m, used in Eq (2). Here, actual concentration ratios $\alpha_{m,0} = 0.3$ (a), 1.0 (b) and 2.0 (c) are assumed. The error is shown for relative GM fractions with φ_{GM} ranging from 0.5 to 0.95. Fig 6d–6f depicts ε as a function of φ_{GM} assuming actual concentration ratios of $\alpha_{m,0} = 0.3$ (d), 1.0 (e) and 2.0 (f). Several values of α_m are considered, ranging from an underestimation equal to -50% to an overestimation of +50% of the actual concentration ratio $\alpha_{m,0}$. We observed that ε increases as the relative fraction φ_{GM} decreases. It is also clear that, for a given $\alpha_{m,0}$, the error tends to be smaller if $\alpha_m > \alpha_{m,0}$ than if $\alpha_m < \alpha_{m,0}$ by the same amount. In other words, it is preferable to overestimate the concentration ratio used in M_2 than to underestimate it (which

Table 2. Measured metabolites α_m-ratio, literature values and concentration estimated using M_2 for 3 T and 7 T.

Metabolite	$\alpha_m \pm \sigma_\alpha$		α_m literature values	$\langle c_{m,2} \rangle \pm$ SEM [mM]		$\langle$CRLB$\rangle \pm$ SEM [%]	
	3 T	7 T		3 T	7 T	3 T	7 T
Asp	1.15 ± 0.12		0.14 [52]	2.3 ± 0.3	1.7 ± 0.6	15 ± 1.8	27.4 ± 12.3 (*)
GABA	0.26 ± 0.06		0.36–1 [19, 52, 53]	2.2 ± 0.7	2.6 ± 0.8	26.5 ± 9.4	10.8 ± 1.9 (*)
Gln	0.41 ± 0.04	0.44 ± 0.04	0.39–0.57 [52, 54]	5.8 ± 0.7	3.7 ± 0.6	8.7 ± 1.2	6.4 ± 1.7 (*)
Glu	0.61 ± 0.02		0.39–0.84 [28, 52, 54]	10.7 ± 1.2	10.8 ± 0.7	4.2 ± 0.6	2.2 ± 0.4 (*)
GSH	0.94 ± 0.05		0.75 [52]	1.5 ± 0.1	1.5 ± 0.3	10.6 ± 1.2	8.8 ± 2.7 (*)
Ins	1.52 ± 0.14		0.72–1 [54]	5.0 ± 0.7	5.3 ± 0.9	3.2 ± 0.4	3.1 ± 0.7
Lac	2.1 ± 0.3		-	0.5 ± 0.1	0.5 ± 0.2	28.3 ± 11.2	21.7 ± 8.3
NAA	0.88 ± 0.03		0.82–1.05 [28, 52, 54, 55]	10.0 ± 0.6	10.5 ± 0.6	3.0 ± 0.4	2.1 ± 0.3 (*)
NAAG	3.8 ± 1.1		1.86–5.4 [52, 54]	0.9 ± 0.2	0.9 ± 0.2	14.8 ± 3.5	9.3 ± 2.5 (*)
PE	0.54 ± 0.07		-	2.8 ± 0.9	2.7 ± 0.8	20.0 ± 9.7	13.9 ± 7.1
Scyllo	1.1 ± 0.33	-	1 [52]	0.3 ± 0.1	-	22.6 ± 7.1	-
Tau	1.2 ± 0.2		0.5 [52]	1.2 ± 0.2	1.3 ± 0.5	29.6 ± 6.9	19.9 ±11.6 (*)
tCho	1.31 ± 0.09		1.33–1.46 [52, 56, 57]	1.7 ± 0.3	1.6 ± 0.2	4.1 ± 0.5	3.9 ± 0.8
tNAA	1.1 ± 0.04		0.96–1.22 [52, 54]	10.8 ± 0.7	11.5 ± 0.7	2	1.7 ± 0.5 (*)
tCr	0.81 ± 0.04	0.82 ± 0.05	0.77 [52]	8.7 ± 0.8	10.1 ± 0.9	2.5 ± 0.5	2 ± 0.4 (*)
Glx	0.54 ± 0.03	0.57 ± 0.02	0.34–0.8 [28, 52]	16.2 ± 1.7	14.1 ± 0.6	4.0 ± 0.6	2.3 ± 0.5 (*)

The metabolite WM-to-GM concentration ratios, α_m-ratio, estimated in this work are shown in the second and third columns. The standard deviation of α_m, σ_α, was calculated using conventional error propagation based on the fitting errors of c_{GM} and c_{WM}. The fourth column contains the range of literature values obtained by both single-voxel MRS or MRS imaging. Notice that the range of literature α_m-ratio values were calculated in this work using the c_{WM} and c_{GM} published in the corresponding reference. In these references, the VOIs contained mostly, but not only, WM or GM; therefore, there is always a certain degree of PVE contamination. Mean metabolite concentrations ± SEM [mM] for 3 T (fifth column) and for 7 T (sixth column), were calculated according to method M_2. CRLB values ± SEM [%] estimated at both 3 T and 7 T are shown in the seventh and eighth columns, respectively. Significant differences in CRLB values at 3 T vs. 7 T are denoted by * ($p < 0.05$).

https://doi.org/10.1371/journal.pone.0286633.t002

was also previously observed by Harris et al. [19]). Note also that the error ε tends to increase more rapidly with decreasing φ_{GM} for the case $\alpha_{m,0} > 1$ (Fig 6f) compared to the case $\alpha_{m,0} < 1$ (Fig 6d). That is to say, metabolites with $\alpha_{m,0} > 1$ tend to be more volatile than those with $\alpha_{m,0} < 1$ when quantified using method M_2 (Eq (2)).

3.5 Comparison of correction methods and field strengths

Fig 7a shows a comparison of the mean and SEM of the metabolite concentrations taken over the whole putamen group, calculated using methods M_1 and M_2, for 3 T (red) and 7 T (blue) scanners. In the case of metabolites where α_m differed significantly from unity, we observed that M_2 led to significantly different concentrations (*, $p < 0.05$) compared to M_1. It is, however, important to note that another factor influencing the significance of the difference between M_1 and M_2 is the inter-subject variability of the metabolite concentration. Notice that the M_2 method for the case of Gln, tCr, and Glx was evaluated using the corresponding separate α_m-ratio values (either 3 T or 7 T), based on the observed significant difference of the $c_{m,1}$ concentration distributions between field strengths. For the rest of the metabolites, the α_m-ratio values obtained using pooled data were used. Regarding the comparison between the scanners, Asp, tNAA, tCr, Glx, and Gln showed a significant difference between the field strengths (#, $p < 0.05$) for both correction methods. The relative difference between the concentrations calculated with M_2 and M_1, $\Delta c_m = 100\% \times (c_{m,2} - c_{m,1})/c_{m,1}$, is plotted in Fig 7b. Fig 7c shows the plot of the corresponding α_m-ratio values for the whole metabolic profile.

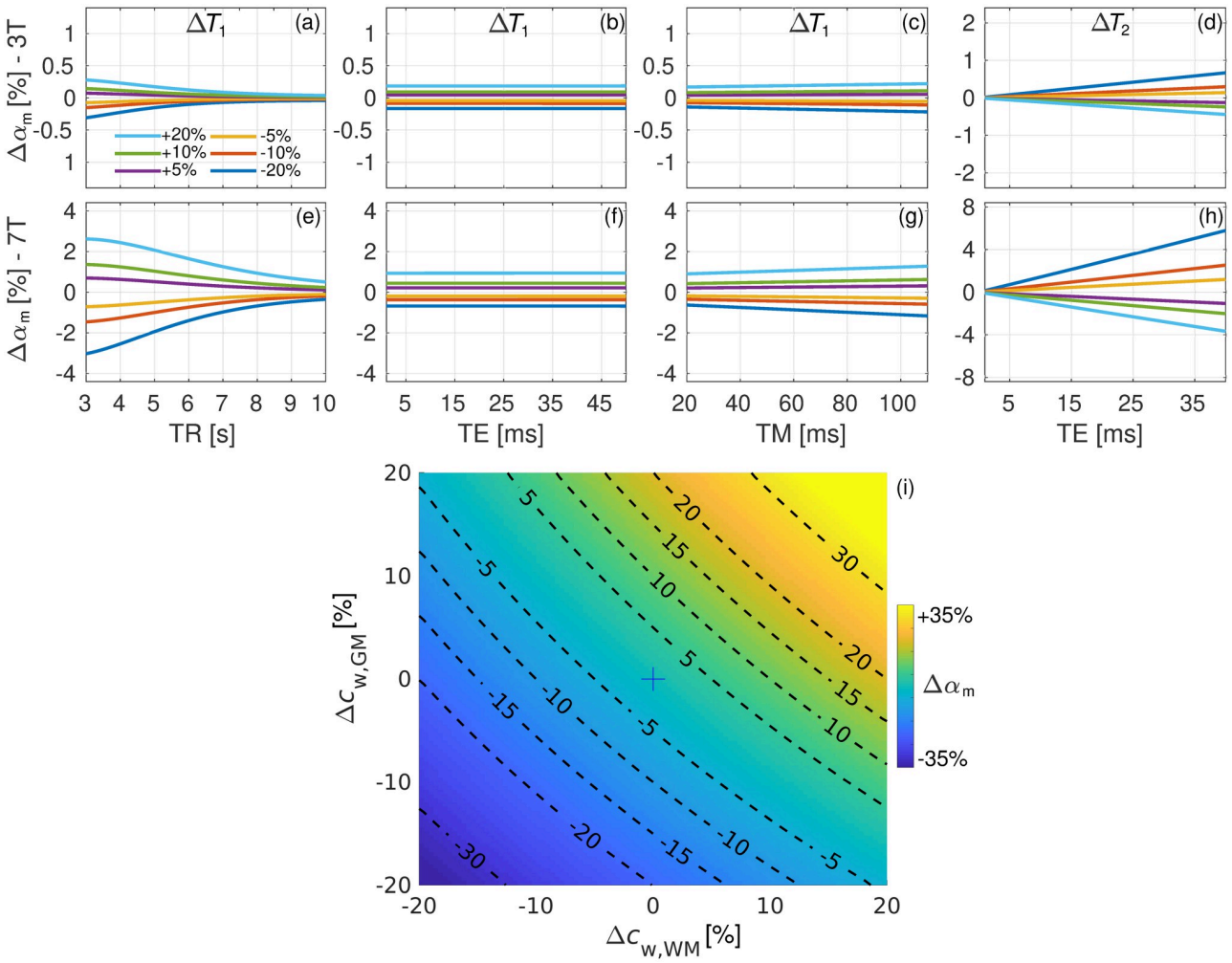

Fig 5. Parameter $\Delta\alpha_m$ as defined in Eq (4) for several values ΔT_1 (a-c, e-g), ΔT_2 (d, h), $\Delta c_{w,WM}$ and $\Delta c_{w,GM}$ (i) ranging from -20% to +20%. For the case of relaxation times, a range of TR, TE, and TM values was considered for 3 T (a-d) and 7 T (e-h) scanners.

https://doi.org/10.1371/journal.pone.0286633.g005

4. Discussion

We have provided a thorough quantification of the metabolic profile of the human putamen in a cohort of healthy, elderly subjects. Although the features covered by the M_1 method have already been broadly discussed in the literature [13, 25, 28, 33, 58], the α_m-ratio method has only been investigated for the case of GABA in a few works [19, 22, 59]. Hence, our secondary goal focused on investigating the α_m-ratio method, with the putamen being the anatomical target. Finally, concentrations quantified at field strengths of 3 T and 7 T were compared as a means of validation.

The data quality for the 3 T and 7 T scanners, as assessed via the linewidth of the unsuppressed water peaks, reflected a strong, positive correlation between the scanners (Fig 2). Furthermore, good spectral quality was achieved throughout the whole study, which is evident in the average (Fig 3) and individual spectra (S2 Fig). Additionally, better B0 shimming was achieved in the case of the occipital, parietal and frontal WM VOIs compared to the putamen VOI, as observed in Fig 2. The most likely explanation is that the difference in the magnetic susceptibility between the putamen and the surrounding WM matter creates large B0 field

Table 3. Summary of Pearson's correlation coefficients analysis for M_1 and M_2.

Metabolite	ρ for $c_{m,1}$ vs. φ_{GM}		ρ for $c_{m,2}$ vs. φ_{GM}	
	3 T	7 T	3 T	7 T
Asp	-0.16 (p = 0.26)		-0.006 (p = 0.97)	
GABA	0.68 (p < 0.001)		0.03 (p = 0.86)	
Gln	0.87 (p < 0.001)	0.88 (p < 0.001)	0.02 (p = 0.94)	0.01 (p = 0.96)
Glu	0.81 (p < 0.001)		0.03 (p = 0.84)	
GSH	0.13 (p = 0.36)		0.002 (p = 0.99)	
Ins	-0.51 (p < 0.001)		0.009 (p = 0.95)	
Lac	-0.62 (p < 0.001)		0.005 (p = 0.97)	
NAA	0.46 (p < 0.001)		0.006 (p = 0.97)	
NAAG	-0.7 (p < 0.001)		0.06 (p = 0.68)	
PE	0.47 (p < 0.001)		0.03 (p = 0.81)	
Scyllo	-0.07 (p = 0.79)	-	-0.004 (p = 0.99)	-
Tau	-0.15 (p = 0.32)		-0.0008 (p = 1.0)	
tCho	-0.44 (p < 0.001)		-0.004 (p = 0.98)	
tNAA	-0.31 (p = 0.025)		0.001 (p = 0.99)	
tCr	0.531 (p = 0.0036)	0.52 (p = 0.0077)	0.009 (p = 0.96)	0.009 (p = 0.96)
Glx	0.84 (p < 0.001)	0.92 (p < 0.001)	0.03 (p = 0.89)	0.04 (p = 0.86)

Pearson's correlation coefficients (ρ) of $c_{m,1}$ and $c_{m,2}$ vs. φ_{GM} and the corresponding p-values, for 3 T and 7 T data. Correlation analysis was performed for pooled (3 T and 7 T) data except for Gln, tCr and Glx, given their significant difference in $c_{m,1}$ distributions between the scanners based on the ANCOVA analysis.

https://doi.org/10.1371/journal.pone.0286633.t003

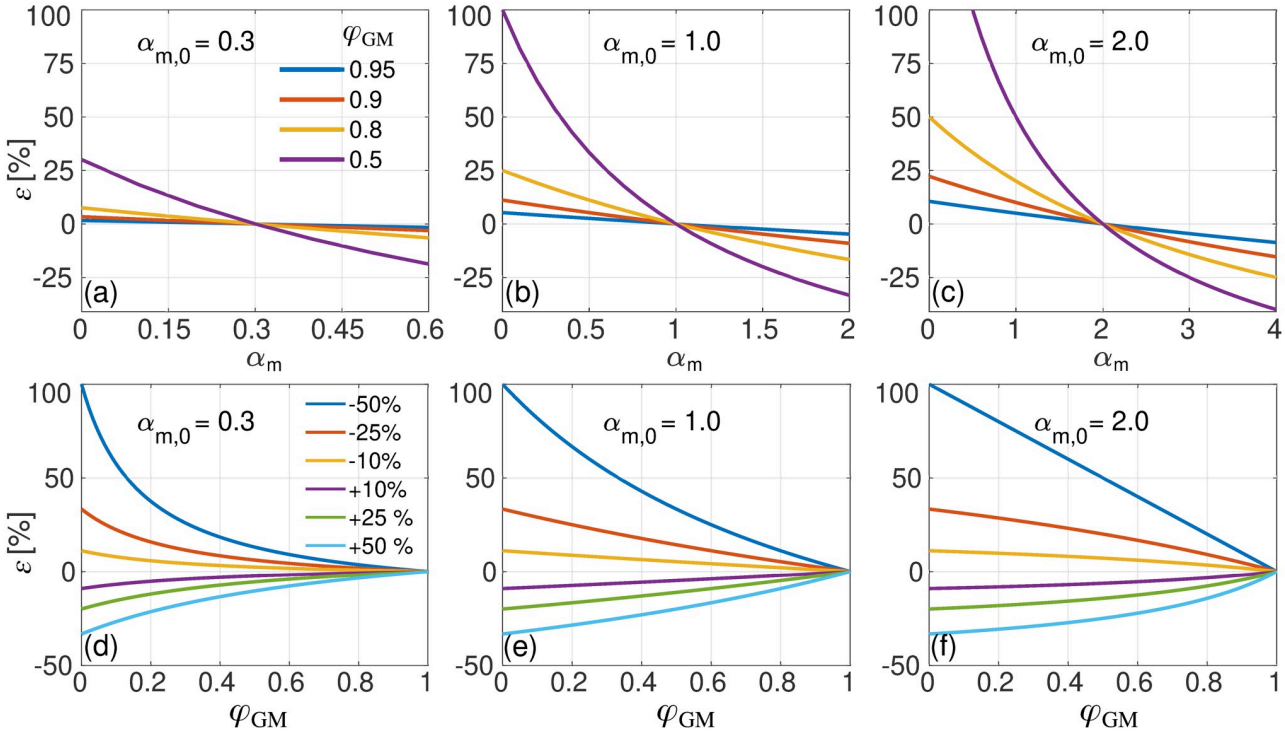

Fig 6. (a-c) Evaluation of the error, ε (Eq 5), in the metabolite concentration as estimated using M_2 vs. α_m, assuming that the used fraction α_m deviates from the actual fraction $\alpha_{m,0}$ = 0.3 (a), 1.0 (b), and 2.0 (c). Several values of the relative fraction φ_{GM} are shown. (d-f) Evaluation of the error, ε, vs. φ_{GM}, for several values of α_m, assuming true values of $\alpha_{m,0}$ = 0.3 (d), 1.0 (e) and 2.0 (f).

https://doi.org/10.1371/journal.pone.0286633.g006

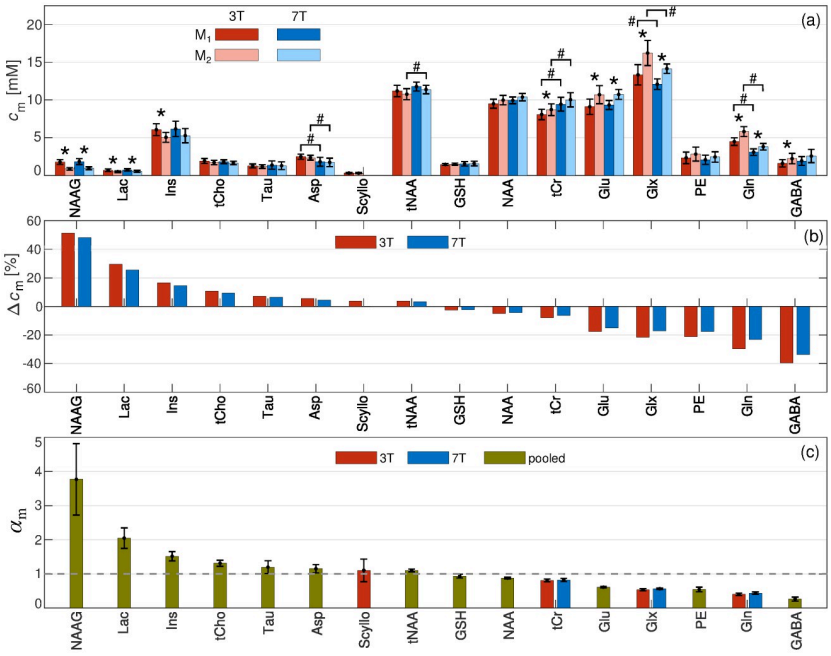

Fig 7. (a) Comparison of the correction methods M_1 and M_2 for 3 T (dark and light red) and 7 T (dark and light blue) scanners. The mean and SEM of the metabolite concentrations across the subjects of the putamen group are shown. A two-sample *t*-test analysis was performed to compare M_1 with M_2 (*, $p < 0.05$). (b) Relative difference in metabolite concentrations between M_1 and M_2 methods, Δc_m. (c) α_m-ratio values were calculated using either pooled data (green), only 3 T data (red) or only 7 T data (blue). Metabolites are ordered in such a way that α_m appears in descending order from left to right. For the case of Gln, tCr and Glx the α_m-ratio values from 7 T are used for ordering purposes.

https://doi.org/10.1371/journal.pone.0286633.g007

distortions [60]. In this work, we have utilised FASTESTMAP for B0 shimming, which optimises shim coils up to second-order. Although it has been demonstrated that the use of higher-order terms in the shimming of the frontal and occipital cortex plays only a marginal role [61], the effect of higher shim orders in other regions, e.g. the putamen, may be more substantial, and therefore, further investigation is required.

The use of STEAM enabled the data acquisition at ultra-short TE, which in turn has the advantage of providing i) high SNR spectra and ii) low spectral distortion of multiplets. The combination of these features facilitated the reliable detection and quantification of 12 metabolites and four total concentrations, as reflected by the low CRLB values [23, 24, 39]. Despite the fact that the mean SNR values were comparable at both fields (as a result of different VOI sizes and number of averages), our results also show that the CRLB values are, in general, lower at 7 T than at 3 T for the putamen [9, 24, 62]. This demonstrates that the simplification of spectral patterns and lower peak overlap at higher field strengths indeed play an important role in the quantification precision, even for comparable SNR values [24]. More specifically, the reduction in the CRLB values for the "mostly singlet" metabolites (e.g. NAA, tCr and tCho) [63] was in the range -5% to -30% for 7 T compared to 3 T. Conversely, the decrease in the CRLB values for the J-coupled metabolites (e.g. GABA, Glu, Gln, Lac, NAAG, PE and Tau) was broader, ranging from -17% for GSH and going up to -48% for Glu and -60% for GABA. In general, the milder improvement in quantification precision with increasing field strength for "mostly singlet" metabolites compared to the large improvement seen in the case of J-coupled metabolites has been previously demonstrated using Monte Carlo simulations [63] and *in vivo* experiments [24, 62, 64]. Furthermore, the behaviour for the particular cases of Ins, which showed almost no decrease in the CRLB values with increasing field strength (-3%), and Asp,

which showed increasing CRLB values, has also been observed in simulations [63] and *in vivo* experiments [24, 62, 64]. Finally, Scyllo was only reliably detected at 3 T, which was similar to other works in the literature where the CRLB worsened with increasing field strength [24, 62, 65] and is most likely due to its intrinsically low concentration.

Conversely, a drawback of short-TE sequences is the presence of strong macromolecular background peaks that complicate spectral fitting [66]. To overcome this, we have included in the LCModel basis sets the macromolecular spectra acquired using the inversion recovery STEAM sequence measured using similar experimental parameters [24, 46]. The validity of using a general macromolecular spectrum is based on the fact that the difference in such spectra between tissue types is negligible [66]. Nevertheless, an investigation using age- and region-specific macromolecular spectra in the basis set is worth considering for future studies.

The short TE and relatively long TR used in our work allowed us to ameliorate a possible bias in α_m due to any potential inaccuracy in the relaxation times used for water and metabolites in Eqs (1) and (2). Indeed, it has been shown that ageing induces changes in the water relaxation times [67–71] as well as in the metabolite relaxation times [72–74]. Hence, the use of single literature values may pose a limitation when studying groups comprising a broad range of ages. The age range covered in this work was 53 to 80. An examination of the literature revealed that, in this age range, the water T_1 in WM can increase by up to roughly 10% in WM [67], whereas the increment in T_2 can be up to nearly 8% [71]. Regarding the putamen, the literature suggests a milder decrease with age of nearly 2% in T_2 [69, 71]. On the contrary, there is some conflicting evidence regarding the age-related changes in the putamen T_1, with some works demonstrating increments with age of roughly 18% [67] while others report no significant changes [68] or even a decrease with age [69]. Given our experimental timings, the analysis shown in Fig 5a–5h demonstrates that a bias of ±20% in the water relaxation times (which englobes the former reported changes and other possible sources of bias) would result in $\Delta\alpha_m < 1\%$ from the values reported here. However, it is evident that in the case of experiments using short TR and/or long TE, the use of age- and anatomy-matched relaxation time values is crucial. In contrast, Fig 5i shows a stronger dependence of $\Delta\alpha_m$ versus a potential bias in $c_{w,WM}$ or $c_{w,GM}$. However, Neeb et al. [29] reported no age dependency for $c_{w,WM}$, whereas for $c_{w,GM}$ a decrease of 0.034% per year was observed. That gives a total reduction of roughly -1.2% in the age range of 53 to 80. Moreover, Taubert et al. [75] also observed a slight reduction in water content in the putamen, although the numbers were not published. Hence, although the effect of ageing on α_m via $c_{w,WM}$ or $c_{w,GM}$ in the studied age range is not expected to be substantial, its investigation in a broader age range should be carefully considered.

The impact of the intrinsic assumption made in Eqs (1) and (2) that the metabolite relaxation times in WM and GM are equal has been previously addressed by Gasparovic et al. [76]. In their work, the authors demonstrate that as the correct equation for accounting for differences in the metabolites relaxation times between WM and GM contains two unknowns, it is not explicitly solvable under conventional experimental designs. Nevertheless, Gasparovic and colleagues use the equation to examine the impact of differing metabolite relaxation times between WM and GM on the estimated concentration for different experimental parameters. For the particular case of NAA at 3 T, they show that an assumption of equal T1/T2 metabolite relaxation times can lead to an error of the order of 6.5–7.8% in the estimated concentration using TR = 1.5 s. and TE = 0.144 s. However, the error was drastically reduced to 0.5% for TR = 6 s and TE = 0.006.

In order to estimate the α_m-ratio values, we first utilised ANCOVA to compare the $c_{m,1}$ vs. φ_{GM} distributions at 3 T and 7 T. A lack of significance in the difference indicated that the $c_{m,1}$ vs. φ_{GM} distributions could be pooled for the estimation of a single α_m-ratio. On the contrary, a significant difference in the $c_{m,1}$ vs. φ_{GM} distributions suggests that the α_m-ratios at 3 T and 7

T could diverge due to reasons other than just differences in the tissue voxel composition. However, even though the $c_{m,1}$ vs. φ_{GM} distributions were significantly different for Gln, tCr, and Glx, the α_m-ratio values were comparable. The α_m-ratios measured here were generally in line with the α_m-ratio values calculated using literature WM and GM metabolite concentrations (Table 2), although some discrepancies were observed. In the case of GABA, for instance, we report a ratio $\alpha_{GABA} = 0.26 \pm 0.06$ whereas the literature range is 0.35–1.0 [19, 52, 53]. This observation is in line with a study by Fahn et al. [77], where it was also reported that the highest GABA levels were found in subcortical regions (e.g. basal ganglia) compared to the cortex in rhesus monkeys. Another example is Ins, for which we obtained a ratio of $\alpha_{Ins} = 1.52 \pm 0.14$, whereas the literature range is 0.44–1.0 [54]. One explanation for these discrepancies could be that the literature values were attained using VOIs positioned in WM and cortical GM, whereas in our study, the VOI mainly contained subcortical GM [52, 54]. Another possible factor is attributed to the age-dependency of the concentration of some metabolites [78–81]. Finally, another aspect could be ascribed to the tissue segmentation approach [19]. However, an investigation of different segmentation approaches was beyond the scope of this work.

Accounting for the α_m-ratio has been shown to have important implications in studies where the subject group includes significant differences in the tissue voxel composition due to brain atrophy, for example [21, 22, 59]. Nevertheless, previous studies have focused on the quantification of GABA, and, to the best of our knowledge, the method has not been applied to other metabolites. In the present work, we have provided a quantification of the α_m-ratio for the whole metabolic profile of the human putamen and surrounding WM. For some metabolites, such as GABA, Gln, Glx, Glu and PE, concentrations in the putamen are clearly larger than in the surrounding WM. Therefore, the inclusion of the α_m-ratio in the quantification via M_2 has a significant effect on the evaluated concentration (Fig 7) [19]. Metabolites, such as tCr, NAA, GSH, Asp, tNAA, Scyllo, Tau, and tCho showed α_m-ratios close to unity, and consequently, no significant differences between $c_{m,2}$ and $c_{m,1}$ were observed except in tCr, which differed significantly between the methods in 3 T data only. For the case of Ins and Lac, the concentration in WM was clearly higher than in GM. However, the case of Ins only showed a significant difference between $c_{m,2}$ and $c_{m,1}$ in 3 T data. This can be explained by the fact that the WM fraction was higher in the 3 T VOI than in the 7 T VOI. Finally, NAAG also showed a higher concentration in WM compared to GM, which resulted in a significant difference between $c_{m,2}$ and $c_{m,1}$ at both field strengths. More generally, the ability of M_2 to remove the dependency of the estimated putamen metabolite profile on the partial volume was further demonstrated via the Pearson's correlation analysis (Table 3). While metabolites showing α_m-ratio values significantly different from unity showed a strong, significant correlation with φ_{GM} when quantified with M_1, the correlation was completely absent when M_2 was used. Hence, identifying metabolites for which α_m-ratio deviates significantly from unity is important.

Contrary to several works in the literature devoted to investigating the advantages and pitfalls of MRS techniques with increasing B0 strengths, which normally utilise matched voxel sizes and/or similar protocol parameters [9, 24, 62, 65], our study included different protocols, especially regarding the voxel size (and therefore the tissue voxel composition). This feature served to investigate the quantification approach when comparing method M_2 to M_1. This validation approach was inspired by the work of Dhamala et al. [25], in which the concentrations measured using three different MRS sequences with different protocol parameters were compared to validate the metabolite concentrations. The rationale behind this approach is that comparable results obtained using different approaches give more confidence in the absolute concentration achieved. Similarly, indistinguishable concentrations measured using different field strengths and/or protocol parameters (including VOI tissue composition) should

strengthen the soundness of the quantified putamen metabolic profile. In our work, the observed difference in Asp, tNAA, tCr, Glx and Gln concentrations between 3 T and 7 T when using method M_1, was still observed for method M_2. Therefore, one can conclude that these differences are not due to the different tissue compositions of the voxels at 3 T and 7 T and other factors, such as different chemical shift displacement errors between the scanners, should be considered.

A context in which the α_m-ratio deserves special attention is functional MRS (fMRS). Given that the observed changes in metabolite concentrations due to activation primarily take place in GM, it is expected that, as per the definition of α_m, changes in α_m will also occur as a result of brain activity. Starting from the derivation of Eq (2) [19], it is trivial to show that the difference between the measured metabolite concentration during activation and the resting-state condition is $\Delta c = f_{GM}\,\Delta c_{GM}$ and therefore $|\Delta c| \leq |\Delta c_{GM}|$. Hence, the change in the metabolite concentration between activation and resting state, as assessed using Eq (2), will show a larger or equal magnitude compared to the change in the measured (i.e. VOI-specific) metabolite concentration. In other words, Eq (2) has the effect of magnifying the change in metabolite concentrations due to brain activation compared to the VOI-specific measured change (Eq (1)). In the particular case of our study, the MRS experiments were performed under resting state conditions, and therefore, there are no physiological reasons to expect variations in the α_m-ratio. However, studies have shown that in the presence of some stimuli, the concentration of metabolites, e.g. Lac, can fluctuate as much as 30% within the VOI [82]. Therefore, a study fully devoted to the investigation of the α_m-ratio within the framework of fMRS is worth considering for future studies.

It is worth mentioning that we have not made use of the tissue-correction approach normalised to the study-specific voxel composition, as originally proposed by Harris et al. (Eq (6) in reference [19]). The reason for this is that we were interested in specifically assessing the absolute metabolic profile of the putamen. That is to say, the metabolic profile of the putamen must not depend on the MRS tissue voxel composition. However, tissue composition normalisation is well advised for cases such as group comparison, especially when brain atrophy is involved [19]. Therefore, given the importance of the former method, a thorough understanding of the α_m-ratio for the whole metabolic profile for the different brain regions becomes paramount and emphasises the importance of our results.

5. Limitations

A limitation of this work is the fact that the metabolite basis sets used in LCModel were simulated using ideal RF pulses. However, while real RF pulses with localisation gradients are preferable, the improvement is not expected to be substantial for the case of STEAM, as shown by Kaiser et al. [83].

A further important limitation of this work is that the tissue water concentration was assumed based on literature values, which normally correspond to the case of healthy, young volunteers. However, it has been shown that the tissue water concentration can be altered, not only in the case of brain pathologies, e.g. hepatic encephalopathy [84], stroke and tumour [85], and cirrhosis [86], but also due to age [29]. Furthermore, the tissue water concentration depends on brain anatomy [87]. Although the impact of age on tissue water content is rather mild [29], increases of nearly 7% in stroke and roughly 10%-15% in tumour tissue have been reported [85]. These changes would result in large deviations in the estimated metabolite concentration and α_m-ratios, as shown in Fig 5i. This drawback could be overcome in future studies by introducing a water mapping technique in the study protocol to assess region- and subject-specific water concentrations [15, 27, 29, 87–91]. More generally, the ideal

experimental setup should pursue the determination of subject- and tissue-specific water relaxation times and concentration [15] as well as metabolite relaxation times.

6. Conclusions

We have investigated a method for the quantification of the neurochemical profile of the brain using MRS, which accounts for differences in the metabolite concentrations of the different tissues comprised in the voxel. The method was applied to quantify the neurochemical profile of the human putamen in a cohort of healthy elderly subjects using STEAM MRS at 3 T and 7 T. The data were then compared to the metabolite concentrations obtained using the conventional correction approach that assumes equal concentration in all tissues. We demonstrate that accounting for differences in the metabolite concentrations between WM and GM leads to significant differences in the estimated metabolite concentration provided that α_m significantly differs from unity. Furthermore, the investigated method was able to remove any dependence of the putamen metabolite concentration on the tissue voxel composition. Finally, not only have we provided a quantification of the neurochemical profile of the human putamen, but also the α_m-ratio of the metabolite concentration profile with the surrounding WM. Our data may potentially serve as a reference for the classification of the degree of metabolic changes in the putamen within the framework of neurodegenerative diseases.

Supporting information

S1 Fig. VOI positioning in the occipital, parietal and frontal WM at 3 T and 7 T.
(DOCX)

S2 Fig. MRS spectra for each of the subjects from the putamen group. Dotted lines denote the subjects for whom the spectra were skipped due to a linewidth greater than 0.07 ppm.
(DOCX)

S1 Table. Mean metabolite concentrations as outputted by LCModel without further corrections.
(DOCX)

S2 Table. Metabolite relaxation times for 3 T and 7 T.
(DOCX)

Acknowledgments

Dedicated to the memory of Prof. Ketevan Kotetishvili.

This study is considered to be part of the doctoral thesis (Dr. rer. medic.) of Ms Ana Gogishvili, Faculty of Medicine, RWTH Aachen University, Germany. We would like to acknowledge E.J. Auerbach and M. Marjanska (Center for Magnetic Resonance Research and the Department of Radiology, University of Minnesota, USA) for the development of the STEAM and FASTESTMAP sequences for the Siemens platform, which was provided by the University of Minnesota under a C2P agreement. We thank Ms Claire Rick for proofreading the manuscript, Dr Jörg Felder for technical assistance, and Dr Seong Dae Yun and Dr Zaheer Abbas for useful discussions.

Author Contributions

Conceptualization: Ana Gogishvili, Ezequiel Farrher, Christopher E. J. Doppler, Michael Sommerauer, N. Jon Shah.

Data curation: Ana Gogishvili, Ezequiel Farrher, Christopher E. J. Doppler, Aline Seger, Michael Sommerauer.

Formal analysis: Ana Gogishvili, Ezequiel Farrher.

Funding acquisition: Christopher E. J. Doppler, Michael Sommerauer, N. Jon Shah.

Investigation: Ezequiel Farrher, Christopher E. J. Doppler, Aline Seger, Michael Sommerauer.

Methodology: Ana Gogishvili, Ezequiel Farrher, Christopher E. J. Doppler, Michael Sommerauer, N. Jon Shah.

Project administration: Christopher E. J. Doppler, Michael Sommerauer, N. Jon Shah.

Resources: Christopher E. J. Doppler, Michael Sommerauer, N. Jon Shah.

Software: Ana Gogishvili, Ezequiel Farrher.

Supervision: N. Jon Shah.

Validation: Ana Gogishvili, Ezequiel Farrher, Christopher E. J. Doppler, Aline Seger, Michael Sommerauer, N. Jon Shah.

Visualization: Ana Gogishvili, Ezequiel Farrher.

Writing – original draft: Ana Gogishvili, Ezequiel Farrher.

Writing – review & editing: Christopher E. J. Doppler, Aline Seger, Michael Sommerauer, N. Jon Shah.

References

1. Martín Noguerol T, Sánchez-González J, Martínez Barbero JP, García-Figueiras R, Baleato-González S, Luna A. Clinical Imaging of Tumor Metabolism with 1H Magnetic Resonance Spectroscopy. Magn Reson Imaging Clin N Am. 2016; 24(1):57–86. Available from: https://doi.org/http%3A//dx.doi.org/10.1016/j.mric.2015.09.002 PMID: 26613876
2. Ali R, Goubran M, Choudhri O, Zeineh MM. Seven-Tesla MRI and neuroimaging biomarkers for Alzheimer's disease. Neurosurg Focus. 2015; 39(5). https://doi.org/10.3171/2015.9.FOCUS15326 PMID: 26646928
3. Graff-Radford J, Kantarci K. Magnetic resonance spectroscopy in Alzheimer's disease. Neuropsychiatr Dis Treat. 2013; 9:687–96. https://doi.org/10.2147/NDT.S35440 PMID: 23696705
4. Seger AD, Farrher E, Doppler CEJ, Gogishvili A, Worthoff WA, Filss CP, et al. Putaminal γ-Aminobutyric Acid Modulates Motor Response to Dopaminergic Therapy in Parkinson's Disease. Mov Disord. 2021;1–6.
5. Martin HL, Teismann P. Glutathione—a review on its role and significance in Parkinson's disease. FASEB J. 2009; 23(10):3263–72. https://doi.org/10.1096/fj.08-125443 PMID: 19542204
6. Marjańska M, McCarten JR, Hodges J, Hemmy LS, Grant A, Deelchand DK, et al. Region-specific aging of the human brain as evidenced by neurochemical profiles measured noninvasively in the posterior cingulate cortex and the occipital lobe using 1H magnetic resonance spectroscopy at 7 T. Neuroscience. 2017; 354(2017):168–77. https://doi.org/10.1016/j.neuroscience.2017.04.035 PMID: 28476320
7. Wijtenburg SA, Rowland LM, Oeltzschner G, Barker PB, Workman CI, Smith GS. Reproducibility of brain MRS in older healthy adults at 7T. NMR Biomed. 2019; 32(2):1–8. https://doi.org/10.1002/nbm.4040 PMID: 30489668
8. de Graaf RA. In Vivo NMR Spectroscopy. Edition 2nd, editor. John Wiley and Sons. Chichester, UK: John Wiley & Sons, Ltd; 2007. 470–472 p. http://doi.wiley.com/10.1002/9780470512968
9. Pradhan S, Bonekamp S, Gillen JS, Rowland LM, Wijtenburg SA, Edden RAE, et al. Comparison of single voxel brain MRS AT 3T and 7T using 32-channel head coils. Magn Reson Imaging. 2015; 33(8):1013–8. Available from: https://doi.org/10.1016/j.mri.2015.06.003 PMID: 26117693
10. Vrenken H, Barkhof F, Uitdehaag BMJ, Castelijns JA, Polman CH, Pouwels PJW. MR spectroscopic evidence for glial increase but not for neuro-axonal damage in MS normal-appearing white matter. Magn Reson Med. 2005; 53(2):256–66. https://doi.org/10.1002/mrm.20366 PMID: 15678547

11. Emir UE, Auerbach EJ, van de Moortele PF, Marjańska M, Uğurbil K, Terpstra M, et al. Regional neurochemical profiles in the human brain measured by 1H MRS at 7T using local B 1 shimming. NMR Biomed. 2012; 25(1):152–60.

12. Kreis R, Ernst T, Ross BD. Absolute Quantitation of Water and Metabolites in the Human Brain. II. Metabolite Concentrations. J Magn Reson Ser B. 1993; 102(1):9–19.

13. Gasparovic C, Song T, Devier D, Bockholt HJ, Caprihan A, Mullins PG, et al. Use of tissue water as a concentration reference for proton spectroscopic imaging. Magn Reson Med. 2006; 55(6):1219–26. https://doi.org/10.1002/mrm.20901 PMID: 16688703

14. Barker PB, Soher BJ, Blackband SJ, Chatham JC, Mathews VP, Bryan RN. Quantitation of proton NMR spectra of the human brain using tissue water as an internal concentration reference. NMR Biomed. 1993; 6(1):89–94. https://doi.org/10.1002/nbm.1940060114 PMID: 8384470

15. Gasparovic C, Neeb H, Feis DL, Damaraju E, Chen H, Doty MJ, et al. Quantitative spectroscopic imaging with in situ measurements of tissue water T1, T2, and density. Magn Reson Med. 2009; 62(3):583–90. https://doi.org/10.1002/mrm.22060 PMID: 19526491

16. Ernst T, Kreis R, Ross BD. Absolute Quantitation of Water and Metabolites in the Human Brain. I. Compartments and Water. J Magn Reson Ser B. 1993; 102(1):1–8.

17. Wilson M, Andronesi O, Barker PB, Bartha R, Bizzi A, Bolan PJ, et al. Methodological consensus on clinical proton MRS of the brain: Review and recommendations. Magn Reson Med. 2019; 82(2):527–50. https://doi.org/10.1002/mrm.27742 PMID: 30919510

18. Hetherington HP, Pan JW, Mason GF, Adams D, Vaughn MJ, Twieg DB, et al. Quantitative 1H spectroscopic imaging of human brain at 4.1 T using image segmentation. Magn Reson Med. 1996; 36(1):21–9. https://doi.org/10.1002/mrm.1910360106 PMID: 8795016

19. Harris AD, Puts NAJ, Edden RAE. Tissue correction for GABA-edited MRS: Considerations of voxel composition, tissue segmentation, and tissue relaxations. J Magn Reson Imaging. 2015; 42(5):1431–40. https://doi.org/10.1002/jmri.24903 PMID: 26172043

20. Gussew A, Erdtel M, Hiepe P, Rzanny R, Reichenbach JR. Absolute quantitation of brain metabolites with respect to heterogeneous tissue compositions in 1H-MR spectroscopic volumes. Magn Reson Mater Physics, Biol Med. 2012; 25(5):321–33.

21. Mikkelsen M, Singh KD, Brealy JA, Linden DEJ, Evans CJ. Quantification of γ-aminobutyric acid (GABA) in 1H MRS volumes composed heterogeneously of grey and white matter. NMR Biomed. 2016; 29(11):1644–55.

22. Porges EC, Woods AJ, Lamb DG, Williamson JB, Cohen RA, Edden RAE, et al. Impact of tissue correction strategy on GABA-edited MRS findings. Neuroimage. 2017; 162(March):249–56. Available from: https://doi.org/10.1016/j.neuroimage.2017.08.073 PMID: 28882635

23. Tkáč I, Starc Z, Choi I, Gruetter R. In Vivo 1H NMR Spectroscopy of Rat Brain at 1 ms Echo Time. Magn Reson Med. 1999; 41:649–56. https://doi.org/10.1002/(sici)1522-2594(199904)41:4<649::aid-mrm2>3.0.co;2-g PMID: 10332839

24. Tkáč I, Öz G, Adriany G, Uğurbil K, Gruetter R. In vivo 1H NMR spectroscopy of the human brain at high magnetic fields: Metabolite quantification at 4T vs. 7T. Magn Reson Med. 2009; 62(4):868–79. https://doi.org/10.1002/mrm.22086 PMID: 19591201

25. Dhamala E, Abdelkefi I, Nguyen M, Hennessy TJ, Nadeau H, Near J. Validation of in vivo MRS measures of metabolite concentrations in the human brain. NMR Biomed. 2019; 32(3):1–15. https://doi.org/10.1002/nbm.4058 PMID: 30663818

26. Provencher SW. Estimation of metabolite concentrations from localized in vivo proton NMR spectra. Magn Reson Med. 1993; 30(6):672–9. https://doi.org/10.1002/mrm.1910300604 PMID: 8139448

27. Neeb H, Zilles K, Shah NJ. A new method for fast quantitative mapping of absolute water content in vivo. Neuroimage. 2006; 31(3):1156–68. https://doi.org/10.1016/j.neuroimage.2005.12.063 PMID: 16650780

28. Gasparovic C, Yeo R, Mannell M, Ling J, Elgie R, Phillips J, et al. Neurometabolite concentrations in gray and white matter in mild traumatic brain injury: An 1H-magnetic resonance spectroscopy study. J Neurotrauma. 2009; 26(10):1635–43. https://doi.org/10.1089/neu.2009.0896 PMID: 19355814

29. Neeb H, Zilles K, Shah NJ. Fully-automated detection of cerebral water content changes: Study of age- and gender-related H2O patterns with quantitative MRI. Neuroimage. 2006; 29(3):910–22. https://doi.org/10.1016/j.neuroimage.2005.08.062 PMID: 16303316

30. Knight-Scott J, Li SJ. Effect of Long TE on T1 Measurement in STEAM Progressive Saturation Experiment. J Magn Reson. 1997; 126(2):266–9. https://doi.org/10.1006/jmre.1997.1171 PMID: 9218348

31. Ethofer T, Mader I, Seeger U, Helms G, Erb M, Grodd W, et al. Comparison of Longitudinal Metabolite Relaxation Times in Different Regions of the Human Brain at 1.5 and 3 Tesla. Magn Reson Med. 2003; 50(6):1296–301. https://doi.org/10.1002/mrm.10640 PMID: 14648578

32. Träber F, Block W, Lamerichs R, Gieseke J, Schild HH. 1H Metabolite Relaxation Times at 3.0 Tesla: Measurements of T1 and T2 Values in Normal Brain and Determination of Regional Differences in Transverse Relaxation. J Magn Reson Imaging. 2004; 19(5):537–45. https://doi.org/10.1002/jmri.20053 PMID: 15112302

33. Larsen RJ, Newman M, Nikolaidis A. Reduction of variance in measurements of average metabolite concentration in anatomically-defined brain regions. J Magn Reson. 2016; 272:73–81. Available from: https://doi.org/10.1016/j.jmr.2016.09.005 PMID: 27662403

34. Brant-Zawadzki M, Gillan GD, Nitz WR. MP RAGE: a three-dimensional, T1-weighted, gradient-echo sequence—initial experience in the brain. Radiology. 1992; 182(3):769–75. Available from: https://doi.org/10.1148/radiology.182.3.1535892 PMID: 1535892

35. Marques JP, Kober T, Krueger G, van der Zwaag W, Van de Moortele PF, Gruetter R. MP2RAGE, a self bias-field corrected sequence for improved segmentation and T1-mapping at high field. Neuroimage. 2010; 49(2):1271–81. Available from: https://doi.org/10.1016/j.neuroimage.2009.10.002 PMID: 19819338

36. Gruetter R, Tkáč I. Field mapping without reference scan using asymmetric echo-planar techniques. Magn Reson Med. 2000; 43(2):319–23. https://doi.org/10.1002/(sici)1522-2594(200002)43:2<319::aid-mrm22>3.0.co;2-1 PMID: 10680699

37. Van De Moortele PF, Akgun C, Adriany G, Moeller S, Ritter J, Collins CM, et al. B1 destructive interferences and spatial phase patterns at 7 T with a head transceiver array coil. Magn Reson Med. 2005; 54(6):1503–18. https://doi.org/10.1002/mrm.20708 PMID: 16270333

38. Metzger GJ, Snyder C, Akgun C, Vaughan T, Ugurbil K, Van De Moortele PF. Local B1+ shimming for prostate imaging with transceiver arrays at 7T based on subject-dependent transmit phase measurements. Magn Reson Med. 2008; 59(2):396–409. https://doi.org/10.1002/mrm.21476 PMID: 18228604

39. Tkáč I, Andersen P, Adriany G, Merkle H, Uurbil K, Gruetter R. In vivo 1H NMR spectroscopy of the human brain at 7 T. Magn Reson Med. 2001; 46(3):451–6. https://doi.org/10.1002/mrm.1213 PMID: 11550235

40. Simpson R, Devenyi GA, Jezzard P, Hennessy TJ, Near J. Advanced processing and simulation of MRS data using the FID appliance (FID-A)—An open source, MATLAB-based toolkit. Magn Reson Med. 2017; 77(1):23–33. https://doi.org/10.1002/mrm.26091 PMID: 26715192

41. Near J, Edden R, Evans CJ, Paquin R, Harris A, Jezzard P. Frequency and phase drift correction of magnetic resonance spectroscopy data by spectral registration in the time domain. Magn Reson Med. 2015; 73(1):44–50. https://doi.org/10.1002/mrm.25094 PMID: 24436292

42. Soher BJ, Semanchuk P, Todd D, Steinberg J, Young K. VeSPA: Integrated applications for RF pulse design, spectral simulation and MRS data analysis. In: Proc Intl Soc Mag Reson Med 19. 2011.

43. Henry PG, Marjanska M, Walls JD, Valette J, Gruetter R, Uğurbil K. Proton-observed carbon-edited NMR spectroscopy in strongly coupled second-order spin systems. Magn Reson Med. 2006; 55(2):250–7. https://doi.org/10.1002/mrm.20764 PMID: 16402370

44. Govindaraju V, Young K, Maudsley AA. Proton NMR chemical shifts and coupling constants for brain metabolites. NMR Biomed. 2000; 13(3):129–53. https://doi.org/10.1002/1099-1492(200005)13:3<129::aid-nbm619>3.0.co;2-v PMID: 10861994

45. Govind V, Young K, Maudsley AA. Corrigendum to Proton NMR chemical shifts and coupling constants for brain metabolites. [NMR Biomed. 13, (2000), 129–153]. NMR Biomed. 2015; 28(7):923–4.

46. Deelchand DK, Marjańska M, Hodges JS, Terpstra M. Sensitivity and specificity of human brain glutathione concentrations measured using short-TE 1H MRS at 7 T. NMR Biomed. 2016; 29(5):600–6. https://doi.org/10.1002/nbm.3507 PMID: 26900755

47. Deelchand DK, Adanyeguh IM, Emir UE, Nguyen TM, Valabregue R, Henry PG, et al. Two-site reproducibility of cerebellar and brainstem neurochemical profiles with short-echo, single-voxel MRS at 3T. Magn Reson Med. 2015; 73(5):1718–25. https://doi.org/10.1002/mrm.25295 PMID: 24948590

48. Bednařík P, Moheet A, Deelchand DK, Emir UE, Eberly LE, Bareš M, et al. Feasibility and reproducibility of neurochemical profile quantification in the human hippocampus at 3T. NMR Biomed. 2015 Jun 1; 28(6):685–93.

49. Visser E, Keuken MC, Douaud G, Gaura V, Bachoud-Levi AC, Remy P, et al. Automatic segmentation of the striatum and globus pallidus using MIST: Multimodal Image Segmentation Tool. Neuroimage. 2016; 125:479–97. Available from: https://doi.org/10.1016/j.neuroimage.2015.10.013 PMID: 26477650

50. Zhang Y, Brady M, Smith S. Segmentation of brain MR images through a hidden Markov random field model and the expectation-maximization algorithm. IEEE Trans Med Imaging. 2001; 20(1):45–57. https://doi.org/10.1109/42.906424 PMID: 11293691

51. Patenaude B, Smith SM, Kennedy DN, Jenkinson M. A Bayesian model of shape and appearance for subcortical brain segmentation. Neuroimage. 2011; 56(3):907–22. https://doi.org/10.1016/j.neuroimage.2011.02.046 PMID: 21352927

52. Hofmann L, Slotboom J, Jung B, Maloca P, Boesch C, Kreis R. Quantitative 1H-magnetic resonance spectroscopy of human brain: Influence of composition and parameterization of the basis set in linear combination model-fitting. Magn Reson Med. 2002; 48(3):440–53. https://doi.org/10.1002/mrm.10246 PMID: 12210908

53. Choi C, Bhardwaj PP, Kalra S, Casault CA, Yasmin US, Allen PS, et al. Measurement of GABA and contaminants in gray and white matter in human brain in vivo. Magn Reson Med. 2007; 58(1):27–33. https://doi.org/10.1002/mrm.21275 PMID: 17659613

54. Pouwels PJW, Frahm J. Regional metabolite concentrations in human brain as determined by quantitative localized proton MRS. Magn Reson Med. 1998; 39(1):53–60. https://doi.org/10.1002/mrm.1910390110 PMID: 9438437

55. Tal A, Kirov II, Grossman RI, Gonen O. The role of gray and white matter segmentation in quantitative proton MR spectroscopic imaging. NMR Biomed. 2012; 25(12):1392–400. https://doi.org/10.1002/nbm.2812 PMID: 22714729

56. Hong D, van Asten JJA, Rankouhi SR, Thielen JW, Norris DG. Implications of the magnetic susceptibility difference between grey and white matter for single-voxel proton spectroscopy at 7 T. J Magn Reson. 2018; 297:51–60. Available from: https://doi.org/10.1016/j.jmr.2018.10.007 PMID: 30359907

57. van de Bank BL, Emir UE, Boer VO, van Asten JJA, Maas MC, Wijnen JP, et al. Multi-center reproducibility of neurochemical profiles in the human brain at 7T. NMR Biomed. 2015; 28(3):306–16.

58. Brief EE, Moll R, Li DKB, MacKay AL. Absolute metabolite concentrations calibrated using the total water signal in brain 1H MRS. NMR Biomed. 2009; 22(3):349–54. https://doi.org/10.1002/nbm.1349 PMID: 19107764

59. Saleh MG, Near J, Alhamud A, van der Kouwe AJW, Meintjes EM. Effects of tissue and gender on macromolecule suppressed gamma-aminobutyric acid. Int J Imaging Syst Technol. 2017; 27(2):144–52.

60. Marjańska M, Auerbach EJ, Valabrègue R, Van de Moortele PF, Adriany G, Garwood M. Localized 1H NMR spectroscopy in different regions of human brain in vivo at 7T: T 2 relaxation times and concentrations of cerebral metabolites. NMR Biomed. 2012; 25(2):332–9.

61. Henning A. Proton and multinuclear magnetic resonance spectroscopy in the human brain at ultra-high field strength: A review. Neuroimage. 2018; 168:181–98. Available from: https://doi.org/10.1016/j.neuroimage.2017.07.017 PMID: 28712992

62. Terpstra M, Cheong I, Lyu T, Deelchand DK, Emir UE, Bednařík P, et al. Test-retest reproducibility of neurochemical profiles with short-echo, single-voxel MR spectroscopy at 3T and 7T. Magn Reson Med. 2016; 76(4):1083–91. https://doi.org/10.1002/mrm.26022 PMID: 26502373

63. Deelchand DK, Iltis I, Henry PG. Improved quantification precision of human brain short echo-time 1H magnetic resonance spectroscopy at high magnetic field: A simulation study. Magn Reson Med. 2014; 72(1):20–5. https://doi.org/10.1002/mrm.24892 PMID: 23900976

64. Bartha R, Drost DJ, Menon RS, Williamson PC. Comparison of the quantification precision of human short echo time 1H spectroscopy at 1.5 and 4.0 Tesla. Magn Reson Med. 2000; 44(2):185–92. https://doi.org/10.1002/1522-2594(200008)44:2<185::aid-mrm4>3.0.co;2-v PMID: 10918316

65. Mekle R, Mlynárik V, Gambarota G, Hergt M, Krueger G, Gruetter R. MR spectroscopy of the human brain with enhanced signal intensity at ultrashort echo times on a clinical platform at 3T and 7T. Magn Reson Med. 2009; 61(6):1279–85. https://doi.org/10.1002/mrm.21961 PMID: 19319893

66. Schaller B, Xin L, Gruetter R. Is the macromolecule signal tissue-specific in healthy human brain? a 1H MRS study at 7 tesla in the occipital lobe. Magn Reson Med. 2014; 72(4):934–40. https://doi.org/10.1002/mrm.24995 PMID: 24407736

67. Cho S, Jones D, Reddick WE, Ogg RJ, Steen Grant R. Establishing norms for age-related changes in proton T1 of human brain tissue in vivo. Magn Reson Imaging 1997; 15(10) 1133–1143. https://doi.org/10.1016/s0730-725x(97)00202-6 PMID: 9408134

68. Okubo G, Okada T, Yamamoto A, Fushimi Y, Okada T, Murata K, et al. Relationship between aging and T1 relaxation time in deep gray matter: A voxel-based analysis. J Magn Reson Imaging. 2017 Sep 1; 46(3):724–31. https://doi.org/10.1002/jmri.25590 PMID: 28152255

69. Jara H, Sakai O, Mankal P, Irving RP, Norbash AM. Multispectral Quantitative Magnetic Resonance Imaging of Brain Iron Stores A Theoretical Perspective. Top Magn Reson Imaging. 2006; 17:19–30. https://doi.org/10.1097/01.rmr.0000245460.82782.69 PMID: 17179894

70. Yeatman JD, Wandell BA, Mezer AA. Lifespan maturation and degeneration of human brain white matter. Nat Commun. 2014; 5:4932. https://doi.org/10.1038/ncomms5932 PMID: 25230200

71. Sedlacik J, Boelmans K, Löbel U, Holst B, Siemonsen S, Fiehler J. Reversible, irreversible and effective transverse relaxation rates in normal aging brain at 3T. Neuroimage. 2014 Jan 1; 84:1032–41. https://doi.org/10.1016/j.neuroimage.2013.08.051 PMID: 24004692

72. Kirov II, Fleysher L, Fleysher R, Patil V, Liu S, Gonen O. Age dependence of regional proton metabolites T2 relaxation times in the human brain at 3 T. Magn Reson Med. 2008; 60(4):790–5. https://doi.org/10.1002/mrm.21715 PMID: 18816831

73. Kreis R, Slotboom J, Hofmann L, Boesch C. Integrated data acquisition and processing to determine metabolite contents, relaxation times, and macromolecule baseline in single examinations of individual subjects. Magn Reson Med. 2005; 54(4):761–8. https://doi.org/10.1002/mrm.20673 PMID: 16161114

74. Jiru F, Skoch A, Wagnerova D, Dezortova M, Viskova J, Profant O, et al. The age dependence of T2 relaxation times of N-acetyl aspartate, creatine and choline in the human brain at 3 and 4T. NMR Biomed. 2016 Mar 1; 29(3):284–92.

75. Taubert M, Roggenhofer E, Melie-Garcia L, Muller S, Lehmann N, Preisig M, et al. Converging patterns of aging-associated brain volume loss and tissue microstructure differences. Neurobiol Aging. 2020 Apr 1; 88:108–18. https://doi.org/10.1016/j.neurobiolaging.2020.01.006 PMID: 32035845

76. Gasparovic C, Chen H, Mullins PG. Errors in 1H-MRS estimates of brain metabolite concentrations caused by failing to take into account tissue-specific signal relaxation. NMR Biomed. 2018 Jun 1; 31(6). https://doi.org/10.1002/nbm.3914 PMID: 29727496

77. Fahn S, Ccote LJ. Regional Distribution of Γ-Aminobutyric Acid (Gaba) in Brain of the Rhesus Monkey. J Neurochem. 1968; 15(3):209–13.

78. Kadota T, Horinouchi T, Kuroda C. Development and aging of the cerebrum: Assessment with proton MR spectroscopy. Am J Neuroradiol. 2001; 22(1):128–35. PMID: 11158898

79. Brooks JCW, Roberts N, Kemp GJ, Gosney MA, Lye M, Whitehouse GH. A proton magnetic resonance spectroscopy study of age-related changes in frontal lobe metabolite concentrations. Cereb Cortex. 2001; 11(7):598–605. https://doi.org/10.1093/cercor/11.7.598 PMID: 11415962

80. Harada M, Miyoshi H, Otsuka H, Nishitani H, Uno M. Multivariate analysis of regional metabolic differences in normal ageing on localised quantitative proton MR spectroscopy. Neuroradiology. 2001; 43 (6):448–52. https://doi.org/10.1007/s002340000513 PMID: 11465755

81. Angelie E, Bonmartin A, Boudraa A, Gonnaud PM, Mallet JJ, Sappey-Marinier D. Regional differences and metabolic changes in normal aging of the human brain: proton MR spectroscopic imaging study. Am J Neuroradiol. 2001 Jan; 22(1):119–27. Available from: http://www.ncbi.nlm.nih.gov/pubmed/11158897 PMID: 11158897

82. Bednařík P, Tkáč I, Giove F, Dinuzzo M, Deelchand DK, Emir UE, et al. Neurochemical and BOLD responses during neuronal activation measured in the human visual cortex at 7 Tesla. J Cereb Blood Flow Metab. 2015 Mar 31; 35:601–10. https://doi.org/10.1038/jcbfm.2014.233 PMID: 25564236

83. Kaiser LG, Young K, Matson GB. Numerical simulations of localized high field 1H MR spectroscopy. J Magn Reson. 2008 Nov; 195(1):67–75. https://doi.org/10.1016/j.jmr.2008.08.010 PMID: 18789736

84. Shah NJ, Neeb H, Kircheis G, Engels P, Häussinger D, Zilles K. Quantitative cerebral water content mapping in hepatic encephalopathy. Neuroimage. 2008 Jul 1; 41(3):706–17. https://doi.org/10.1016/j.neuroimage.2008.02.057 PMID: 18456518

85. Oros-Peusquens AM, Loução R, Abbas Z, Gras V, Zimmermann M, Shah NJ. A Single-Scan, Rapid Whole-Brain Protocol for Quantitative Water Content Mapping With Neurobiological Implications. Front Neurol. 2019; 10(December):1–22. https://doi.org/10.3389/fneur.2019.01333 PMID: 31920951

86. Winterdahl M, Abbas Z, Noer O, Thomsen KL, Gras V, Nahimi A, et al. Cerebral water content mapping in cirrhosis patients with and without manifest HE. Metab Brain Dis. 2019 Aug 15; 34(4):1071–6. https://doi.org/10.1007/s11011-019-00427-y PMID: 31089866

87. Abbas Z, Gras V, Möllenhoff K, Keil F, Oros-Peusquens AM, Shah NJ. Analysis of proton-density bias corrections based on T1 measurement for robust quantification of water content in the brain at 3 Tesla. Magn Reson Med. 2014; 72(6):1735–45. https://doi.org/10.1002/mrm.25086 PMID: 24436248

88. Abbas Z, Gras V, Möllenhoff K, Oros-Peusquens AM, Shah NJ. Quantitative water content mapping at clinically relevant field strengths: A comparative study at 1.5 T and 3 T. Neuroimage. 2015; 106:404–13. Available from: https://doi.org/10.1016/j.neuroimage.2014.11.017 PMID: 25463455

89. Schall M, Zimmermann M, Iordanishvili E, Gu Y, Shah Jon N, Oros-Peusquens AM. A 3D two-point method for whole-brain water content and relaxation time mapping: Comparison with gold standard methods. PLoS One. 2018; 13(8):1–21. https://doi.org/10.1371/journal.pone.0201013 PMID: 30161125

90. Shah NJ, Ermer V, Oros-Peusquens AM. Measuring the Absolute Water Content of the Brain Using Quantitative MRI. In: Magnetic Resonance Neuroimaging, Methods in Molecular Biology 711,. 2011. p. 29–64. https://doi.org/10.1007/978-1-61737-992-5_3 PMID: 21279597

91. Neeb H, Ermer V, Stocker T, Shah NJ. Fast quantitative mapping of absolute water content with full brain coverage. Neuroimage. 2008; 42(3):1094–109. https://doi.org/10.1016/j.neuroimage.2008.03.060 PMID: 18632287